Journal of Inorganic Biochemistry 223 (2021) 111549

Contents lists available at ScienceDirect

Journal of Inorganic Biochemistry

journal homepage: www.elsevier.com/locate/jinorgbio

Synthesis, characterization of ruthenium(II), nickel(II), palladium(II), and platinum(II) triphenylphosphine-based complexes bearing an ONS-donor chelating agent: Interaction with biomolecules, antioxidant, *in vitro* cytotoxic, apoptotic activity and cell cycle analysis

Shadia A. Elsayed [a,*], Hagar E. Badr [a], Armando di Biase [b], Ahmed M. El-Hendawy [a,*]

[a] Chemistry Department, Faculty of Science, Damietta University, New Damietta 34517, Egypt
[b] Dipartimento di Chimica, Università degli Studi di Milano, via C. Golgi 19, 20133 Milano, Italy

ARTICLE INFO

Keywords:
Metal complexes
Cytotoxicity
ct DNA
tRNA
BSA
Apoptosis

ABSTRACT

Four new transition metal complexes, $[M(PPh_3)(L)]\cdot CH_3OH$ (M = Ni(II) (**1**), Pd(II) (**2**)) $[Pt(PPh_3)_2(HL)]Cl$ (**3**) and $[Ru(CO)(PPh_3)_2(L)]$ (**4**) (H_2L = 2,4-dihydroxybenzaldehyde-*S*-methyldithiocarbazate, PPh_3 = triphenylphosphine) have been synthesized and characterized by elemental analyses (C, H, N), FTIR, NMR (^1H, ^{31}P), ESI-MS and UV–visible spectroscopy. The molecular structure of (**1**) and (**2**) complexes was confirmed by single-crystal X-ray crystallography. It showed a distorted square planar geometry for both complexes around the metal center, and the H_2L adopt a bi-negative tridentate chelating mode. The interaction with biomolecules *viz.*, calf thymus DNA (ct DNA), yeast RNA (tRNA), and BSA (bovine serum albumin) was examined by both UV–visible and fluorescence spectroscopies. The antioxidant activity of all compounds is discussed on basis of $DPPH^{\bullet}$ (2,2-diphenyl-1-picrylhydrazyl) scavenging activity and showed better antioxidant activity for complexes compared to the ligand. The *in vitro* cytotoxicity of the compounds was tested on human (breast cancer (MCF7), colon cancer (HCT116), liver cancer (HepG2), and normal lung fibroblast (WI38)) cell lines, showing that complex (**1**) the most potent against MCF7 and complex (**4**) against HCT116 cell lines based on IC_{50} and selective indices (SI) values. So, both complexes were chosen for further studies such as DNA fragmentation, cell apoptosis, and cell cycle analyses. Complex (**1**) induced MCF7 cell death by cellular apoptosis and arrest cells at S phase. Complex (**4**) induced HCT116 cell death predominantly by cellular necrosis and arrested cell division at G2/M phase due to DNA damage.

1. Introduction

cis-Platin is the first platinum-based drug used for the treatment of different types of cancer in clinics and is considered as a precursor for other metallotherapeutic drugs such as oxaliplatin, carboplatin [1]. Since the discovery of *cis*-platin, its efficacy is evidenced in diverse types

Abbreviations: ^{1}HNMR, Proton nuclear magnetic resonance; ^{31}PNMR, Phosphorus-31 nuclear magnetic resonance; ARP, Antioxidant reducing power; BSA, Bovine serum albumin; ct DNA, Deoxyribonucleic acid from calf thymus; DMF, Dimethyl formamide; DMSO, Dimethyl sulfoxide; DPA, Diphenylamine; DPPH, 2,2-diphenyl-1-picryhydrazyl; EB, Ethidium bromide; EC_{50}, Effective concentration; ESI-MS, Electron Spray Ionization mass spectroscopy; Et_2O, diethyl ether; F, Fluorescence; *fa*, Fractional accessible protein fluorophore; FTIR, Fourier-transform infrared spectroscopy; H_2L, 2,4-dihydroxybenzaldehyde-*S*-methyldithiocarabzate; HCT116, Human colon cancer; HepG2, Human liver cancer; HPLC, High Performance Liquid Chromatography; HSA, Human serum albumin; IC_{50}, Half maximal inhibitory concentration; K_a, Effective quenching constant for the accessible fluorophore; K_{app}, Apparent binding constant; K_b, Intrinsic binding constant; K_q, Dynamic or collision quenching constant; K_{sv}, Stern-Volmer constant; KP1019, [indazolium *trans*-[tetrachloride bis-(Hindazole) ruthenate(III)]; KP1339, (sodium trans-[tetrachlorobis(1H-indazole)ruthenate(III)]); LMCT, Ligand-to-metal charge transfer; MCF7, Human breast cancer; MLCT, Metal-to-ligand charge transfer; MTT, 3-(4,5-dimethylthiazol−2-yl)-2,5-diphenyltetrazolium bromide; NA, Nucleic acid; NAMI-A, [imidazolium trans- [tetrachlorido(DMSO)(imidazole)ruthenate(III)]; PBS, Phosphate buffered saline; PI, Propidium iodide; PDT, photodynamic therapy; PPh_3, Triphenylphosphine; SAR, Structure activity relationship; SI, Selective index; tRNA, Transfer ribonucleic acid; WI38, Human normal lung fibroblast; ε, Extinction coefficient..

* Corresponding authors.
E-mail addresses: shadia.elsayed@du.edu.eg (S.A. Elsayed), amelhendawy@du.edu.eg (A.M. El-Hendawy).

https://doi.org/10.1016/j.jinorgbio.2021.111549
Received 7 April 2021; Received in revised form 12 July 2021; Accepted 15 July 2021
Available online 21 July 2021

of cancer including ovarian, colorectal, lung, and bladder cancers [2]. On the other hand, its toxicity, serious side effects, and drug resistance property have limited its usage in the clinic [3,4]. From this point, researchers dedicated their efforts to developing platinum and non-platinum metal-based drugs using the advantage of *cis*-platin (clinical use) with new strategies to improve the pharmacological properties and elucidating the mechanism of action of the developed drugs [5]. In addition to *cis*-platin and its derivatives, many metal complexes were found to be potential anticancer agents, such as ruthenium [6], palladium [7], and nickel [8]. The structure-activity relationship (SAR) is an important factor to be taken into consideration while designing an anticancer drug [9]. It explains the relationship between the molecular structures and their biological activity [10], which enables determining the structure or chemical group responsible for the biological effect [11]. Then, the structure can be modified to enhance the bioactivity of the compounds. Due to the resemblance between the coordination geometry of Pt(II), Pd(II) and Ni(II) complexes, palladium and, nickel complexes have received considerable interest, due to the lesser side effect and resistance therapies [7,12]. Platinum is most effective than palladium due to ligand exchange kinetics, as palladium complexes readily dissociate in solution (10^5 times faster than Pt), giving very active species that are unable to reach the biological target such as DNA and RNA and reduce the biological activity [13]. Hence, the structure reactivity relationship plays an important role to design more stable Pd (II) and Ni(II) complexes by introducing strong chelating agents, a bulky ligand such as PPh_3 [7,14], or strongly coordinating nitrogen ligand [15] to overcome the rapid aquation process of theses complexes. From square planar to octahedral complexes (Platinum to ruthenium), inorganic and organometallic ruthenium (II/III) complexes are believed to exhibit promising antitumor activity. Ruthenium(III) complex, sodium *trans*-[tetrachlorobis(1H-indazole) ruthenium(III)]) (KP1339) is currently developed for clinical investigation [16–18], and Ru(II)-polypyridyl compound (TLD − 1433) has recently entered a human clinical trial as PDT (photodynamic therapy) agent for bladder cancer [19].

The unique properties of ruthenium complexes come from their chemistry, it has variable oxidation states (+II to +IV), slow ligand-exchange kinetics as well as octahedral geometry that allows the structure diversity [20]. It has been also reported that ruthenium complexes are less toxic, highly efficient, and selective against specific types of tumors due to their strong affinity to bind to biomolecules (DNA/RNA and bovine serum albumin (BSA) [18,21–23]. The mechanism of action of ruthenium complexes to exert the antitumor effect mainly depends on the nature of the ligand, complexes, and uncoordinated sites present in the coordination sphere of the metal center [24]. Mechanism of action may include inhibition of metastasis [25], binding to DNA and proteins [26], apoptotic cell death, and production of reactive species [27].

Ligand design also has great importance in the development of anticancer agents. S-alkyl and S-aryl dithiocarbazate Schiff bases are an important class of biologically active chelating agents. They contain NS-donors (hard/soft atoms) within a thioamide (thione-thiol) moiety similar to those of thiosemicarbazones [28]. Their flexible properties can be also modified incorporating different substituents [29]. This characteristic improves their chelating ability by forming a stable chelate with five or six-membered rings when linked to the metal ion improving their structural stability as well as biological activity [30,31]. On the other hand, phosphine-based ligands are ligands of biological interest including antitumor, antibacterial, and antifungal properties [32]. They can form complexes with varieties of metal ions, such as Ni (II), Pd(II), Pt(II), and Ru(II) with valuable bioactivities [7,26,33]. In particular, Pd(II)/Ni(II)-PPh_3-based complexes, to reduce their higher lability to ligand exchange of Ni(II) and Pd(II) centers [7].

Nucleic acids (DNA/RNA) and proteins are attractive targets for potential therapeutics. So the interaction of transition metals with those biomolecules is essential to design any efficient metal-based anticancer drugs [34]. However, the binding of transition metals with nucleic acids and protein may induce organ toxicity and other undesirable side effects, *i.e.* cisplatin can induce *in vivo* nephrotoxicity and genotoxicity [35]. This may be attributed to excessive generation of free radicals by the cisplatin inside the cell as well as intra-strand cross-link DNA by the cisplatin in healthy cells [36]. That interaction may cause DNA damage in vital organs, subsequently the appearance of secondary cancers [37]. So, it is important to innovate new metal-based anticancer drugs with antioxidant properties to reduce organ toxicity through the free radical. Also, the *in vivo* studies must be excessively done on the new metal-based anticancer agents to avoid organ toxicity danger.

In this paper, due to the interesting properties of both dithiocarbazate and PPh_3 ligand, we have synthesized and characterized four new complexes of 2,4-dihydroxybenzaldehyde-*S*-methyldithiocarabzate (H_2L) with Ni(II), Pd(II), Pt(II), and Ru(II) bearing PPh_3 ligand; [Ni (PPh_3)(L)]·CH_3OH (**1**), [Pd (PPh_3)(L)]·CH_3OH (**2**), [Pt (PPh_3)$_2$(HL)]Cl (**3**) and [Ru(CO) (PPh_3)$_2$ (L)] (**4**). We report their solution stability, calf thymus (ct DNA)/yeast RNA (tRNA) and BSA binding properties, *in vitro* anticancer activity against human normal and cancer cell lines. Furthermore, DNA fragmentation, apoptotic activity, and cell cycle arrest indicating that (**1**, **4**) are promising metallotherapeutic candidates.

2. Experimental

2.1. Materials

The starting materials, $NiCl_2.6H_2O$, K_2PdCl_4, K_2PtCl_4 (Alfa Aesar), $RuCl_3.xH_2O$ (Pressure Chemicals), 2,4-dihydroxybenzaldehyde (Fischer Scientific), Deoxyribonucleic acid sodium salt from calf thymus (ct DNA), yeast tRNA (Sigma), bovine serum albumin BSA (Biomark, 98.5%) and HPLC grade solvents were used as received. The complexes [Ni(PPh_3)$_2$Cl$_2$] [38], [M(PPh_3)$_2$Cl$_2$] (M = Pd(II), Pt(II)] [39], [RuHCl (CO)(PPh_3)$_2$] [40] and *S*-methyldithiocarbazate [41] were prepared as described in literature. All chemicals used for DNA fragmentation and flow cytometry are from Sigma. The reagents, Roswell Park Memorial Institute (RPMI)1640 medium, MTT (3-(4,5-dimethylthiazol-2-yl)-2,5-diphenyltetrazolium bromide) and dimethyl sulfoxide (DMSO) (Sigma Co., St. Louis, USA), Fetal Bovine serum (GIBCO, UK). The cell lines, Human (WI38), Colorectal carcinoma (HCT116), Mammary gland breast cancer (MCF7) and Hepatocellular carcinoma (HePG2) were obtained from ATCC *via* Holding company for biological products and vaccines (VACSERA), Cairo, Egypt.

2.2. Methods

FT-IR spectra were recorded in the range of 4000–400 cm^{-1} on JASCO 4100 FTIR spectrophotometer from KBr pellet. NMR (^1H and ^{31}P) spectra were acquired on Bruker 400 using d_6-DMSO as a solvent. ESI-MS spectra were performed on Thermo Fisher LCQ Fleet ion trap mass spectrometer equipped with HPLC UltiMate™ 3000 system. Elemental analyses were done at the Microanalysis unit, Cairo University, Egypt. The UV–Vis spectra of the compounds (in DMSO) were recorded by JASCO V 630 using a quartz cuvette with 1 cm path-length at 298 K in the range of 200–900 nm. Spectrofluorimeter (model 6285, UK) was used for fluorescence excitation and emission spectra (200–700 nm). Molar conductance values were determined using 10^{-3} M solution of complexes in DMF using CM-1 K portable conductivity meter. Microplate reader (ELX800, USA) is used for cytotoxic study in MTT assay. The single-crystal X-ray diffraction experiment was performed on a Bruker Smart APEX II CCD diffractometer with graphite monochromated Mo-Kα radiation (l = 0.71073 Å) [42] (Section 1.1, Electronic Supporting Information (ESI†).

2.3. Synthesis

2.3.1. Preparation of 2,4-dihydroxybenzaldehyde-S-methyldithiocarbazate ligand (H_2L)

An ethanolic solution of 2,4-dihydroxybenzaldehyde (1.38 g, 10 mmol, 10 mL) and *S*- methyldithiocarbazate [41] (1.22 g,10 mmol, 10 mL) were mixed and refluxed for 4 h in presence of drops of glacial acetic acid. The resulting yellow solution was concentrated to one-half volume and allowed to cool to room temperature. The yellow crystalline product was filtered, washed twice with ethanol, and dried under *vacuo*. Yield: 71%. M. p.: 210–212 °C. Anal. Calc. for $C_9H_{10}N_2O_2S_2$ (%): C, 44.6; H, 4.1%; N, 11.6%. Found: C, 44.5; H, 4.0; N 11.4%. FT-IR (cm^{-1}) in KBr: ν(O—H) 3429 b, 3296 m; ν(N—H) 3118 w; ν(C=N) 1629 m; ν(C—O) 1218 m, ν(N—N) 1097 m; ν(C=S) 1025 m;(C—S) 844 m. ^{1}H NMR (400 mHz, DMSO-d_6, δ ppm, *J* Hz): δ 2.52 (s, 3H, SCH_3), δ 6.29 (s, 1H, H3), δ 6.33(d, $J = 1.2$ Hz, 1H, H5), δ 7.47(d, $J = 8.0$ Hz, 1H, H6); δ 8.4(s, 1H, —CH=N); δ 10.07(s, 1H, 4-OH); δ10.25(s, 1H, 2-OH); δ 13.22 (s, 1H, NH). UV–Vis (DMSO, 1.66×10^{-5} M): λ_{max} (nm) (ε, M^{-1}. cm^{-1}): 312 (6807), 361 (35240) 377(25783).

2.3.2. Preparation of complexes

2.3.2.1. [Ni(PPh$_3$)(L)]·CH$_3$OH (1). To a methanolic solution of H_2L (0.242 g, 1 mmol), [$NiCl_2(PPh_3)_2$] [38] (0.653 g, 1 mmol) was added. The mixture was refluxed for 3 h and the resulting orange solution was concentrated to one third volume followed by addition of small amount of diethylether (1 mL). The orange crystals suitable for X-ray crystallography were collected by filtration, carefully washed by methanol and diethylether then dried *in vacuo*. Yield: 78%. M. p.: 140–142 °C. Anal. Calc. for $C_{28}H_{27}N_2NiO_3PS_2$ (%): Calcd: C, 56.7; H, 4.6; N, 4.7%. Found: C, 56.6; H, 4.4; N 4.5%. FT-IR (cm^{-1}) in KBr: ν(O—H) 3386 b; ν(C=N) 1618 s; ν(C=N)$_{new}$ 1585 m; ν(N—N) 1025 m; ν(C—S) 845 m; ν(C—O)$_{phenolic}$ 1228 m; ν(Ni—P) 587w; ν(Ni—O) 532 m; ν(Ni—N) 437w; ν(PPh_3) 1069 m,745 m. ^{1}H NMR (400 mHz, DMSO-d_6, δ ppm, *J* Hz): δ 2.50 (s, 3H, SCH_3); δ 6.23(d, $J = 2.2$, 1H, H5); δ 5.78(d, 1H, H3); δ 7.24 (d, $J = 2.0$, 1H, H6); δ7.244–7.7(m, 5H, Ph); δ 8.589(s, 1H,— CH═N); δ 9.88(s, 1H, 4-OH). ESI-MS (*m/z*): Calcd.: 560.03 ([Ni(L)(PPh_3)]), Found: 582.79 ([Ni(L)(PPh_3) + Na]$^+$). UV–Vis (DMSO, 1.66×10^{-5} M): λ_{max} (nm) (ε, M^{-1}. cm^{-1}): 306 (30662), 367 (28132), 384 (32349) and 408 (24518). Molar conductivity (10^{-3} M, DMF, Λ_M):2.0 $\Omega^{-1}cm^2mol^{-1}$.

2.3.2.2. [Pd(PPh$_3$)(L)]·CH$_3$OH (2). The ligand (H_2L) ((0.12 g, 0.5 mmol) was dissolved in methanolic solution containing KOH (5 mL, 0.5 mmol). [$PdCl_2(PPh_3)_2$] [39] (0.35 g, 0.5 mmol) was added to the above solution. The reaction mixture was refluxed for 3 h during which the orange precipitate obtained was filtered off, wash with methanol, followed by diethylether, and then dried in vacuum. The filtrate was left at room temperature for slow evaporation, orange crystals suitable for X-ray crystallography were obtained, washed with methanol and diethylether. Yield: 81%. M. p.: 156–158 °C. Anal. Calc. for $C_{28}H_{27}N_2O_3PPdS_2$, Calcd.: C, 52.46; H, 4.25; N, 4.37%. Found. C, 52.42; H, 4.02; N 4.25%. FT-IR (cm^{-1}) in KBr: ν(O—H) 3412,3283 b; ν(C=N) 1600 s; ν(N—N) 1072 s; ν(C—S) 839 s; ν(C—O)$_{phenolic}$ 1215 s; ν(Pd—P) 588 w; ν(Pd—O) 530 w; ν(Pd—N) 476 m; ν(PPh_3) 979 s,749 m. ^{1}H NMR (400 mHz, DMSO-d_6, δ ppm, *J* Hz): δ 2.56 (s, 3H, SCH_3); δ 4.12 (s,1H, OH (methanol)); δ 5.99 (s,1H, H3); δ 6.24 (d, $J = 2.16$ Hz, 1H, H5); δ 7.44 (d, $J = 4.4$ Hz, 1H, H6); δ 7.55–7.63 (m, 15H, Ph); δ 8.57(s, 1H, —CH=N); δ 9.96(s, 1H, 4-OH). ESI-MS (*m/z*): Calcd.: 607.99 ([Pd(L)(PPh_3)]), Found: 609.01 ([Pd(L)(PPh_3) + H$^+$]). UV–Vis (DMSO, 1.66×10^{-5} M): λ_{max} (nm) (ε, M^{-1}. cm^{-1}): 308 (13012), 350 (9759), 396 (10542). Molar conductivity (10^{-3} M, DMF, Λ_M): 2.0 $\Omega^{-1}cm^2$ mol^{-1}.

2.3.2.3. [Pt(PPh$_3$)$_2$(HL)]Cl (3). To an ethanolic solution of H_2L (0.12 g, 0.5 mmol), [$PtCl_2(PPh_3)_2$] [39] (0.395 g, 0.5 mmol) was added. The mixture was refluxed for 3 h. and the resulting yellow solution was concentrated to one third volume then left for slow evaporation and the yellow precipitate was filtered off, washed with diethyl ether, then dried *in vacuo*. Yield 75%. M. p.:170–172 °C. Anal. Calc. for $C_{45}H_{39}ClN_2O_2P_2PtS_2$, Calcd.: C, 54.24; H, 3.95; N, 2.81%. Found. C, 54.0; H, 3.63; N 2.51%. FT-IR (cm^{-1}) in KBr: ν(O—H) 3283 b; ν(C=N) 1603 s; ν(C=N)$_{new}$ 1556 s; ν(N—N) 1060 s; ν(C—S) 839 s; ν(C—O)$_{phenolic}$ 1252 s; ν(Pt—P) 565 w; ν(Pt—O) 504 w; ν(Pt—N) 430 m; ν(PPh_3) 998, 747 m. ^{1}H NMR (400 mHz, DMSO-d_6, δ ppm, *J* Hz): δ 2.34 (s, 3H, SCH_3); δ 6.43(s,1H, H3); δ 6.22(d, $J = 2.16$ Hz, 1H, H5); δ 6.44(d, $J = 4.4$ Hz, 1H, H6); 7.18–7.70 (m, 30H, Ph); δ 8.53(s, 1H, —CH=N); δ 10.60(s, 1H, 4-OH); δ 10.72(s,1H,2-OH). ^{31}P NMR (162 mHz, DMSO-d_6, δ ppm): δ 2.84 (d, $^2J_{PP} = 81.85$ Hz), δ 23.76 (d, $^2J_{PP} = 70.60$ Hz). ESI-MS (*m/z*): Calcd.: 960.15 ([Pt(HL)(PPh_3)$_2$]$^+$), Found: 962.64 ([Pd(HL)(PPh_3)$_2$ + 2H$^+$]). UV–Vis (DMSO, 1.66×10^{-5} M): λ_{max} (nm) (ε, M^{-1}. cm^{-1}): 370 (9217), 417 (8675). Molar conductivity (10^{-3} M, DMF, Λ_M): 42 $\Omega^{-1}cm^2mol^{-1}$.

2.3.2.4. [Ru(CO)(PPh$_3$)$_2$ (L)] (4). The ligand (H_2L) (0.242 g, 1 mmol) was dissolved in benzene-ethanol mixture (5:1 *v*/v) and [RuHCl(CO)(PPh_3)$_3$] [40] (0.952 g, 1 mmol) was added. The mixture was heated refluxed for 5 h. The resulting orange solution was concentrated under reduced pressure then petroleum ether was added to collect the precipitate. The yellowish orange product was filtered off, washed with Et_2O, and dried under *vacuo*. Yield 62%. M. p.: 160–162 °C. Anal. Calc. for $C_{46}H_{38}N_2O_2S_2$ RuP, Calcd.: C, 61.8; H, 4.28; N, 3.13%. Found. C, 61.60; H, 4.02; N, 3.20%. FT-IR (cm^{-1}) in KBr: ν(O—H) 3387 b; ν(C=N) 1625 s; ν(N—N) 1031 s; ν(C —S) 850 w; ν (C—O)$_{phenolic}$ 1216 m; ν(Ru—P) 587w; ν(Ru—O) 515 w; ν(Ru—N) 462 w; ν(PPh3) 1031, 744 m; ν (C=O) 1937 s. ^{1}H NMR (400 mHz, DMSO-d_6, δ ppm, *J* Hz): δ 2.51 (s, 3H, SCH_3); δ7.236–7.45 (m, 30H, Ph); δ 7.51 (s, 1H, H3); δ7.591(d, 1H, H6); δ 8.24 (s, 1H, —CH=N); δ10.12 (s, 1H, 4-OH). ^{31}P NMR (162 mHz, DMSO-d_6, δ ppm): δ 29.31(s, 1P), 36.26 (s, 2P). ESI-MS (*m/z*): Calcd.: 894.08 [Ru(L)(CO)(PPh_3)$_2$], Found: [Ru(L)(CO)(PPh_3)$_2$+ H$^+$]. UV–Vis (DMSO, 1.66×10^{-5} M): λ_{max} (nm) (ε, M^{-1}. cm^{-1}): 350 (11446), 395 (13313). Molar conductivity (10^{-3} M, DMF, Λ_M): 10 $\Omega^{-1}cm^2mol^{-1}$.

2.4. Solution stability

Study the stability of the complexes in aqueous media is essential to evaluate the biological activity of any metallodrug [43]. A stock solution of 10^{-3} M of each complex was prepared in DMSO (to improve solubility). The sample solutions were prepared by dilution of stock with phosphate-buffered saline (PBS): pH 7.4, 137 mM NaCl, 2.7 mM KCl, 10 mM Na_2HPO_4 and 1.8 mM K_2HPO_4). The stability of complexes (1.66×10^{-5} M) was carried out in (1.6% DMSO/PBS *v*/v). The absorption spectra of the complexes were measured with increasing time (over 24 h) at room temperature.

2.5. Biological applications

2.5.1. Interaction with biomolecules

The interaction studies of biomolecules (ct DNA, tRNA and BSA) were performed in Tris-HCl buffer (pH = 7.2, 5 mM Tris-HCl + 50 mM NaCl). The ctDNA and tRNA concentrations were determined spectrophotometrically at 260 nm ($\varepsilon = 6600$ M^{-1} cm^{-1} for ct DNA) and ($\varepsilon = 7700$ M^{-1} cm^{-1} for tRNA) [44], whereas the concentration of BSA was determined at 280 nm ($\varepsilon = 66{,}433$ M^{-1} cm^{-1}). The required concentrations of the test samples were prepared by dissolving the compound in a minimum amount of DMSO, then completed to the required volume with Tris buffer (1% DMSO/buffer). All the measurements were carried out at room temperature.

2.5.1.1. Absorption studies. The binding affinity of biomolecules (ctDNA, tRNA) towards metal complexes was investigated using UV–visible spectroscopy. Various concentrations of ctDNA (0–140 μM)/

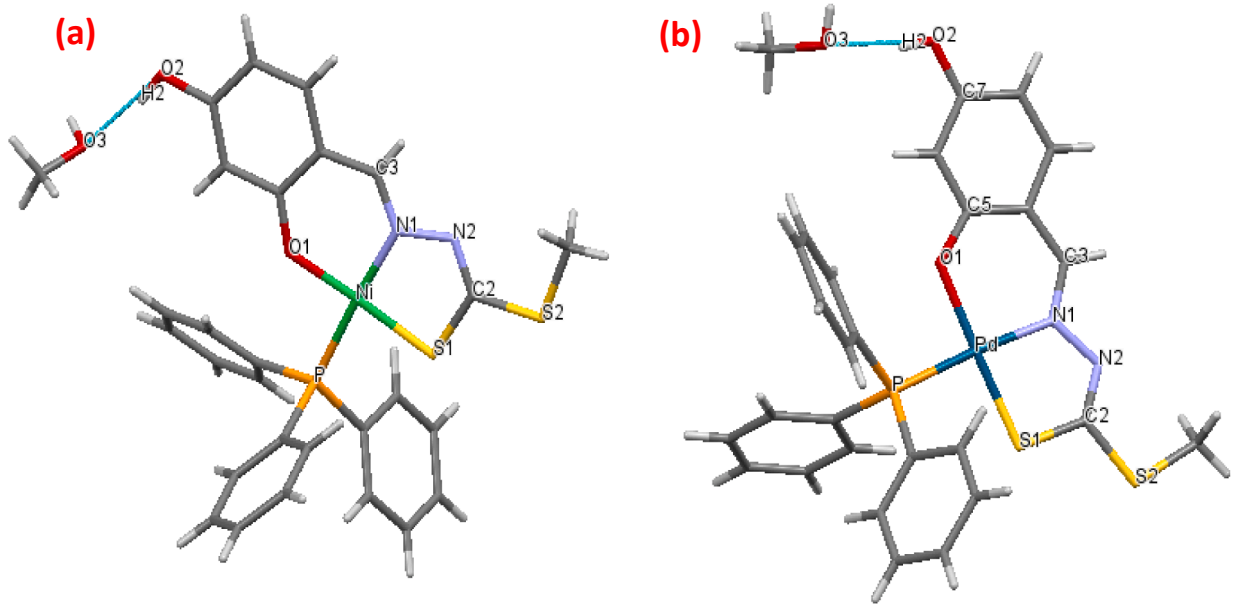

Fig. 1. Molecular structures for (a) $[Ni(PPh_3)(L)]\cdot CH_3OH$ (**1**) and (b) $[Pd(PPh_3)(L)]\cdot CH_3OH$ (**2**).

tRNA (0–45 μM) were added to a fixed concentration of the test compound 70 μM for ct DNA and 45 μM for tRNA. The absorption spectra were measured at 300–500 nm. Tris buffer was used as a blank, and an equivalent amount of ct DNA/tRNA was added to the reference cell to cancel the absorbance of ctDNA/tRNA.

2.5.1.2. Emission study. As the complexes has no fluorescent properties, fluorescence emission spectra of the ligand and its complexes were studied by pretreating the nucleic acid (ctDNA or tRNA) with ethidium bromide (EB) ([ctDNA] = 50 μM, [tRNA] = 80 μM, [EB] = 5 μM in Tris-HCl buffer. Different concentrations of test compounds (0–100 μM) were added to the EB/DNA adduct. The emission was measured at 300–600 nm and the reduction in fluorescence intensity was recorded at 590 nm. The quenching constant was evaluated by employing the Stern-Volmer equation [45].

2.5.2. BSA interaction studies

2.5.2.1. Absorption studies. The BSA-complexes interaction was also determined spectrophotometrically by keeping the concentration of BSA constant (15 μM) with adding different concentrations of test compound (0–30 μM). The absorption spectra were recorded in the range 300–500 nm after 5 min incubation period.

2.5.2.2. Emission study. The quenching emission of BSA tryptophan residues was depicted using the ligand and complexes as quenchers. To a fixed concentration of BSA (50 μM) in Tris-HCl buffer, varying concentrations of quencher (0–50 μM) were added, and the emission intensity was measured after a 5 min incubation period. The fluorescence emission spectra were scanned from 300 to 500 nm (excitation at 295 nm). To determine the quenching parameters of the complexes for BSA, Stern Volmer equations [46] were used.

2.6. Antioxidant activity by DPPH• (2,2-diphenyl-1-picrylhydrazyl) radical scavenging assay

The free radical scavenging activity was determined as reported in the literature [47]. Various concentrations of the test compounds (25–600 μM) and reference compound (ascorbic acid as a standard) were prepared in 2.0 mL of DMSO. Then mixed with 1 mL of DPPH in DMSO. The resulting solution was incubated in dark at room temperature for 30 min before spectrophotometric measurement at 517 nm. The DPPH• scavenging activity percent was determined using Eq. (1):

$$\%\text{DPPH scavenging activity} = \frac{A_c - A_s}{A_c} \times 100 \quad (1)$$

Where A_c and A_s are the absorbances in the presence and absence of the test compound, respectively. The antioxidant activity is expressed based on IC_{50} value and other antioxidant parameters: antioxidant reducing power (ARP), effective concentration (EC_{50}), stoichiometry, and the number of reduced DPPH have been also determined [48].

2.7. In vitro cytotoxic activity assay

The cytotoxic activity of the synthesized compounds was evaluated to determine the inhibitory effects of compounds on cell growth using MTT assay as depicted in (Section 1.2, ESI†).

2.8. Anticancer mechanism

2.8.1. Quantitative analysis of DNA fragmentation

DNA fragmentation by the complexes (**1**) on MCF7 and (**4**) on HCT116 cell lines was analyzed calorimetrically by diphenylamine (DPA) reaction as explained in Section 1.3, ESI†).

2.8.2. Cell apoptosis by flow cytometry

The cell death mode of MCF7 cells by complex (**1**) and HCT116 cells by complex (**4**) line has been performed by annexin V-FITC/PI (propidium iodide) assay (Section 1.4, ESI†).

2.8.3. Cell cycle analysis

The effect of complexes (**1**) and (**4**) on the DNA content by cell cycle progression was assessed using MCF7 and HCT116, respectively (Section 1.5, ESI†).

3. Results and discussion

3.1. Synthesis

Synthesis and characterization details of the ligand and its complexes

Table 1
Selected bond lengths (Å) and bond angles (°) for nickel(II) (**1**) and palladium(II) (**2**) complexes.

	(1)	(2)
Bond lengths (Å)		
M–S1	2.1475(6)	2.2455(6)
M–O1	1.8536(16)	2.0192(5)
M–N1	1.8808(18)	2.0112(16)
M–P	2.2173(6)	2.2759(6)
C2–N2	1.275(3)	1.275(2)
C2–S1	1.743(2)	1.752(2)
C2–S2	1.752(2)	1.7514(9)
Bond angles (°)		
O1–M–P	88.97(5)	91.28(4)
P–M–S1	89.89(2)	92.314(19)
S1–M–N1	86.64(5)	84.12(5)
N1–M–O1	94.54(7)	92.38(1)
O1–M–S1	176.74(6)	175.45(5)
P–M–N1	176.44(6)	175.91(5)

Table 2
Hydrogen bonding parameters for complexes (**1**) and (**2**).

D—H···A	Symmetry	D—H (Å)	H···A (Å)	D···A (Å)	D—H···A (°)
(1)					
(i) O···H and S···H contacts					
O2–H2···O3	x,3/2–y,–1/2 + z	0.775	2.005	2.762	165.66
C18–H24···S2	x,3/2–y,1/2 + z	0.93	2.924	3.684	139.91
(ii) C···H contacts					
O2–H2•••C28	x,y,z	0.775	2.854	3.568	154.39
C3–H3•••C10	2–x,2–y,1–z	0.93	2.802	3.668	155.04
(2)					
(i) O•••H and S•••H contacts					
O2–H2•••O3	x,3/2–y,–1/2 + z	0.81	1.971	2.771	168.97
C18–H18•••S2	x,y,z	0.93	2.97	3.707	137.16
(ii) C•••H contacts					
O3–H3A•••C13	–1 + x,3/2–y,–1/2 + z	0.82	2.748	3.509	155.1
C3–H3•••C10	1–x,1–y,1–z	0.93	2.857	3.726	156.2

have been mentioned in the experimental Section 2.3 (Synthesis). All synthesized compounds are stable in air, insoluble in water, but fairly soluble in DMSO and DMF, and partially soluble in CH_2Cl_2 and CH_3CN. The complexes (**1**), (**2**), and (**4**) showed lower molar conductance values (2.0–10.0 $\Omega^{-1}cm^2mol^{-1}$) which indicated the non-electrolytic nature of the complexes, whereas complex (**3**) has a value of 42 $\Omega^{-1}cm^2mol^{-1}$ indicating 1:1 electrolytic behavior [49].

3.2. Characterization

3.2.1. Molecular structure

Suitable crystals for X-ray diffraction analysis for nickel(II) and palladium(II) complexes $[M(L)(PPh_3)_3].(CH_3OH)$ (M = Ni (**1**), M = Pd (**2**)) were obtained by slow evaporation of their methanolic solutions. Crystallographic data of complexes (**1**) and (**2**) are listed in (Table S1, ESI†) and their molecular structures are shown (Fig. 1a and b). The ligand 2,4-dihyroxybenzaldehyde *S*-methyl dithiocarbazate (L^{2-}) coordinates to Ni(II) or Pd(II) centers in a bi-negative tridentate manner through phenolic oxygen O1, azomethine N1, and thiolate sulfur S2, forming stable five- or six-membered chelate rings. The nickel or palladium center adopts a slightly distorted square planar geometry with bond angles; O1–Ni–P 88.97 (5)°, P–Ni–S1 89.89 (2)°, S1–Ni–N1 86.64 (5)° and N1–Ni–O1 94.54 (7)° of the sum 360° and the angles; O1–Ni–S1 176.74 (6) and P–Ni–N1 176.44 (6)° near the ideal angle 180°. Similar related bond angles (Table 1) are found for palladium(II) complex (**2**). Bond angles with a square planar coordination environment of Ni(II) and Pd(II) are in agreement with that found in the literature [50,51]. The donor atoms O1, N1, and S1 form the tridentate ligand (H_2L), and the phosphorous atom P of PPh_3, occupies the square plane. For complexes (**1**) and (**2**), the data depicted in Table 1 of bond lengths M – X (M = Ni(II), Pd(II); X = O, N, S, P) are similar to those reported for related nickel(II) and palladium(II) complexes [50,52] The C2–N2 bond (1.275(3)Å)(**1**), (1.275(2)Å)(**2**) as the usual C═N bond length [53,54]. The bond length C2–S1 1.743(2) Å for (**1**) and 1.752(2) Å for (**2**) is the same for the single bond C2–S2 1.752(2)(**1**) 1.7514(9)Å (**2**). This is close to that found for similar related O,N,S- donor ligands chelated in their thiolate form [50,54], where the thiol form is also characterized by the fact that the hydrazinic nitrogen N1 is not bonded to any hydrogen atom. The selected bond parameters are listed in Table 1.

The data of specific contacts O•••H, S···H and C···H of the intermolecular hydrogen bonding interactions characterized in the lattice for complexes (**1**) and (**2**) are presented in Table 2. Each molecule of the complex is connected with a strong hydrogen bond between O3 of CH_3OH solvent and H2 of the free hydroxyl group (d_H(H2···O3) = 2.005 Å (**1**), 1.971 Å (**2**)). The distances d_H(O···H) are shorter than the maximum values of 2.72 Å for the van der Waals radii of hydrogen and oxygen atoms and considered for any contact [55]. The molecules are interconnected *via* S2 atom from one molecule and H24(**1**) or H18(**2**) of the other neighboring one, with a weaker interaction C18–H24(H18)··· •S2 d_H(H24(H18)···•S2) = 2.924 Å (**1**), 2.97 Å (**2**). This is similar to that observed in related O,N,S- metal complexes [56–58]. The molecules form parallel planes which are constructed through C10 (PPh_3) in a plane and H3(L^{2-}) of the other plane the contact C3–H3···C10 (d_H(H3···C10) = 2.802 Å (**1**), 2.857 Å (**2**)). In each complex ((**1**) or (**2**)), the molecules are also specifically contacted through C28(CH_3OH) and H2(2-OH), d_H(H2···C28) = 2.854 Å (**1**) or through C13(PPh_3) and H3A (CH_3OH), d_H(H3A···C13) = 2.748 Å (**2**). These lattice contacts are shown in (Fig. S1a,b, ESI†).

3.2.2. Vibrational spectra

The infrared spectral data of the ligand and its complexes have been identified and presented in the experimental Section 2.3. The FTIR spectrum of the free ligand (H_2L) (Fig. 2a), showed its distinctive bands at 3429 and 3118 cm^{-1} which are assigned to ν(O—H) and ν(N—H) stretching vibrations, respectively. In addition, the presence of ν(C=S) stretching vibration at 1097 cm^{-1}, suggests the presence of thione form (HN–C = S) of the free ligand (Schem1a). This phenomenon is also supported by the absence of ν(S—H) at *ca.* 2500 cm^{-1} [48,59]. In the FTIR spectra of complexes (**1**), (**2**) and (**4**), the ν(O—H) and ν(N—H) bands disappeared, and the ν(C—O) band shifted to higher frequency [60,61] (1227–1252 cm^{-1}) as compared to free ligand (1218 cm^{-1}). This result ascertained the involvement of phenolic oxygen (2-OH) in coordination after deprotonation [60]. The coordination *via* azomethine nitrogen ν(C=N) was indicated by the shift of this band to lower frequency in the spectra of the complexes in the (1600–1625 cm^{-1}) region. This is also supported by the shift of ν(N—N) to lower frequency (1027–1060 cm^{-1}) compared to those of the parent ligand (1097 cm^{-1}). The absence of ν(C=S) band at 1025 cm^{-1} in the ligand is replaced by a lower frequency band (839–850 cm^{-1}) for ν(C – S) [62] in complexes along with the appearance of a new strong azomethine band in 1556–1580 cm^{-1} region due to the formation of (C═N – N = C – S^-) moiety (Scheme 1c), this confirms that the ligand coordinates to the metal center through the deprotonated thiol sulfur (Scheme 1b). This concludes that the ligand acts as a bi-negative tridentate ONS-donor through deprotonated phenolic oxygen, azomethine nitrogen, and thiolate sulfur as shown in (Fig. 2b, as a representative example).

Another coordination mode was exhibited by platinum(II) complex (**3**), where there is no significant shift in ν(O—H) bands, while ν(N—H)

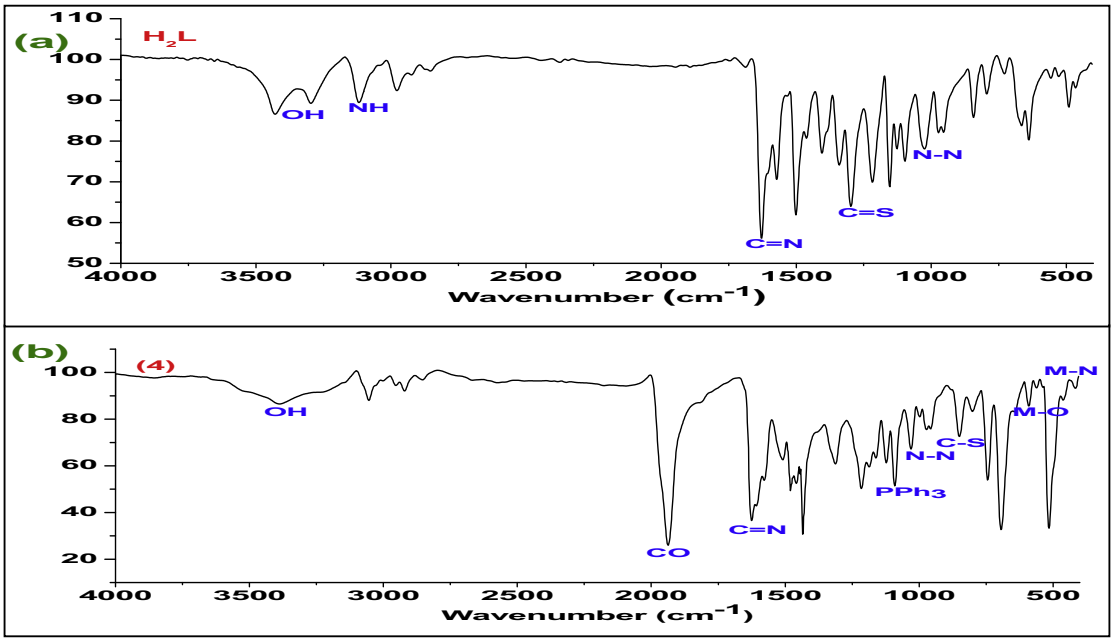

Fig. 2. FT-IR spectra of **(a)** ligand (H_2L) and **(b)** [Ru(CO)$(PPh_3)_2$ (L)] complex (**4**).

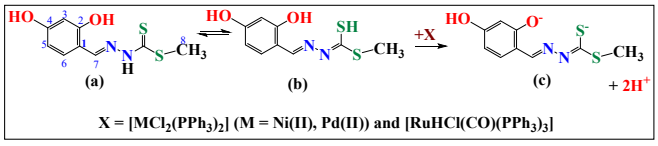

Scheme 1. Tautomeric forms of H_2L ligand; (a) thione and (b) thiol; (c) ionic form.

band disappeared, and a shift to a lower frequency for ν(C=N) was found together with new bands display for ν(C=N) and ν(C—S) as in complexes (**1**), (**2**) and (**4**). This confirms the mono-negative bi-dentate (HL) manner of the ligand as NS-donor through azomethine nitrogen and thiol sulfur (Scheme 1b). In all complexes, the new bands observed at 1091–1097 and 692–694 cm^{-1} are designated to ν(P-Ph) stretching vibrations [63], while the bands appeared at 565–586 cm^{-1} due to 504–532 and 430–476 nm are due to ν(M – P), ν(M – N) and ν(M – N), respectively [64,65]. In Ru(II) complex (**4**), the strong band observed at 1937 cm^{-1} is characteristic for ν(CO). The presence of CH_3OH molecule in the structure of the complex (**2**) is defined by the band at 3597 cm^{-1} and that of complex (**1**) is obscured by the broad band at *ca.* 3500 cm^{-1}. The FTIR spectra of the complexes (**1**)–(**3**) are presented in (Fig. S2a–c, ESI†).

3.2.3. NMR spectra

All ^1H NMR spectral data and their assignments of H_2L ligand and its complexes are stated in the experimental section (2.1) and (Fig. S3a–e, ESI†). The ^1H NMR spectrum of the ligand shows singlets at δ13.22, 10.25, 10.07, 8.40, 6.29, and 2.52 due to NH, 2-OH, 4-OH, CH = N, 3-H, and S-CH_3 protons, respectively [48,60]. The two doublets occurred at δ 6.33 (*J*=1.2 Hz) and δ 7.47 (*J* = 8.0 Hz) are assigned to 5-H and 6-H respectively. The absence of SH signal at ~4.0 ppm, confirms the thione moiety of the ligand (Scheme 1a). In ^1H NMR spectra of the complexes (**1**), (**2**) and (**4**), the NH and 2-OH signals disappeared upon coordination indicating the deprotonation before the coordination. Furthermore, the coordination of azomethine nitrogen is confirmed by the downfield or upfield shift (8.24–8.61 ppm) of azomethine proton (CH=N) [66]. The splitting of the CH resonance of azomethine protons may be due to the nuclear quadrupolar effect [67,68]. Thus, the ^1H NMR

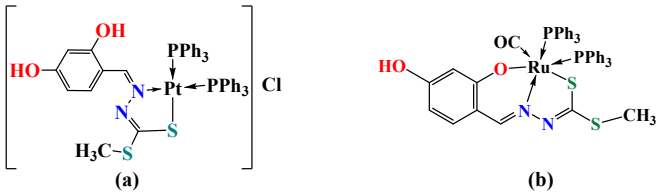

Fig. 3. Proposed structure of (a) [Pt$(PPh_3)_2$(HL)]Cl (**3**) and (b) [Ru(CO)$(PPh_3)_2$(L)] (**4**).

data are constituent with a bi-negative tridentate behavior as ONS-chelating donor for all complexes except for that for platinum(II) (**3**), where NH signal disappeared and the 2-OH signal remain unaltered. This indicates that the ligand coordinates to the Pt(II) center in a mono-negative bidentate manner through thiol sulfur and azomethine nitrogen as NS-donor (Fig. 3a). The triphenylphosphine protons are located in their expected position at δ7.18–7.70 ppm [63]. The ^{31}P NMR spectrum of Pt(II) complex (**3**), shows two doublets at δ 2.70 and 23.48, which indicates the presence of two magnetically different P-atoms coordinated to platinum(II), corresponding to four satellite signals of the Pt(II) ion [69]. For Ru(II) complex (**4**) (Fig. 3b) two signals at 29.0 and 36.33 ppm are shown, indicating the presence of two coordinated triphenylphosphine groups in *cis*-configuration [70].

3.2.4. Mass spectra

Electron Spray Ionization mass (ESI-MS) is a valuable technique for molecular weight determination in coordination compounds. The ESI-MS spectra of the complexes (**1**)–(**4**) are shown in (Fig. S4a–d, ESI†). Their molecular ion peaks [M^+] are in good agreement with the proposed chemical structure. The positive ion ESI-mass spectrum of [Ni(L)(PPh_3)].CH_3OH complex (**1**) shows fragmentation patterns attributed to subsequent degradation of the complex. The signal at *m/z* = 582.79 (Calcd. 583.02, 100%) and 298.92 (Calcd. 297.94, 12%) ascribed to [Ni(L)(PPh_3) + Na]$^+$ and [Ni(L) + H]$^+$, respectively. In addition, the signal located at *m/z* = 1144.23 (Calcd. 1120.06) with relative abundance 100%, attributes to [Ni(L)$(PPh_3)]_2$ + Na]$^+$, and assigned to association of two molecules. The positive ion ESI-mass spectrum of [Pd(PPh_3)(L)]·CH_3OH complex (**2**) shows molecular ion peak at *m/z* = 609.01 (Calcd. 607.99) with a relative abundance of 100% corresponds to [Pd

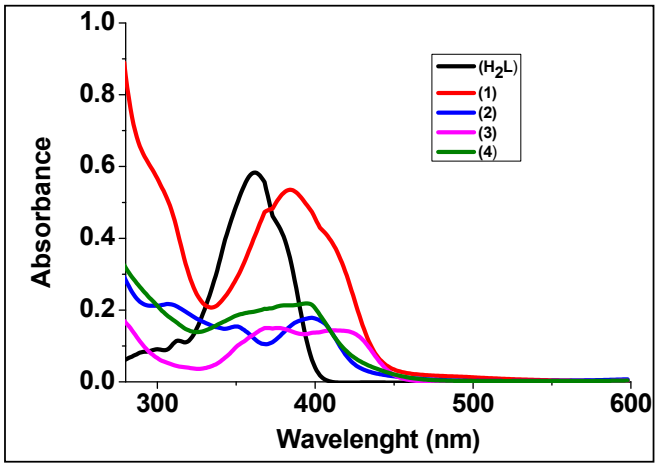

Fig. 4. Electronic spectra of ligand (H_2L) and complexes (**1**)–(**4**) in 1.6×10^{-5} M DMSO.

$(L)(PPh_3) + H]^+$, while in negative ion mode the base peak signal showed up at 607.32 with relative abundance 100% corresponds to $[Pd(PPh_3)(L)\text{-}H]^-$and the second fragment located at 345.16 (345.91, 20%) due to $[Pd(L)\text{-}H]^-$ fragment. The positive ion ESI-mass spectrum of $[Pt(HL)(PPh_3)_2]Cl$ complex (**3**), shows its molecular ion peak at m/z = 962.64 (Calcd. 960.15 with relative abundance 10%) is assigned to $[Pt(PPh_3)_2(HL)]^+$. The other fragment observed at m/z = 698.01 (100%, Calcd. 698.06) is attributed to $[Pt(HL)(PPh_3)]^+$ arising from the loss of one PPh_3 ligand. The positive ion ESI-mass spectrum of $[Ru(CO)(PPh_3)_2(L)]$ complex (**4**) show the first signal at m/z = 895.15 with relative abundance 100% (Calcd. 894.08) assigned to $[Ru(CO)(PPh_3)_2(L) + H]^+$. The second signal appeared at m/z = 633.0 (8%, Calcd. 631.99) is attributed to $[Ru(CO)(PPh_3)(L) + H]^+$ which correspond to the cation formed by missing of PPh_3 ligand.

3.2.5. Electronic spectra and magnetic susceptibility measurements

The magnetic susceptibility measurements revealed that all complexes are diamagnetic with square planar geometry for Ni(II), Pd(II), and Pt(II) complexes which assigned to their (d^8) configuration [71] and low spin (d^6, $S = 0$) for Ru(II) complex [48,54]. The UV–visible spectra of the ligand and its complexes (**1**)–(**4**) were measured for 1.6×10^{-5} M in DMSO solution at room temperature in the 200–600 nm range. The electronic spectrum of the ligand shows absorption bands in 290–377 nm which are assigned to π-π* and n-π* transitions that resulted from azomethine and thiocarbonyl moieties [72,73]. In the electronic spectra of the complexes, these bands were shifted into higher wavelength (redshift) 307–450 nm along with the appearance of a new band in 385–420 nm due to metal-to-ligand charge transfer (MLCT) due to the coordination of metal (II) ion with the azomethine nitrogen and thiol sulfur [74,75]. The d-d transition bands of the complexes obscured due to their relatively low extinction coefficient compared to ligand-to-metal charge transfer (LMCT) or MLCT [76]. The electronic spectra measurements are shown in (Fig. 4 and Table S2, ESI†).

3.2.6. Solution stability

Study the stability of metal complexes in solution is an essential step while evaluating their interaction with biomolecules and anticancer activity [43]. As the anticancer agents are usually introduced into the bloodstream, it is worth studying their stability in aqueous media. For example, it is reported that hydrolysis has a positive influence on the anticancer activity of ruthenium(II) and platinum(II) complexes by activating the DNA binding [77,78]. Hence, the solution stability of the complexes (**1**)–(**4**) was studied by UV–Vis spectroscopy in phosphate-buffered saline (pH = 7.4) containing 1% DMSO over a time period of 24 h (Fig. S5, ESI†). The complexes displayed an increase of absorbance during the first hour near 360 and 400 nm attributed to fluctuation or modification of the original compounds, then the data obtained up to 24 h shows a decrease in absorbance with no significant changes in band positions indicating substantial stability of the complexes in buffer-DMSO solution [74,79]. Complex (**3**) shows a slight spectral change at λ = 430 nm which may simply result from the solvent exchange (DMSO or H_2O) with chloride ion.

4. Biological applications

4.1. Interaction with biomolecules (ct DNA and tRNA and BSA)

In classical studies, DNA was known as the major target to design any anticancer drugs.Recently, RNA also not less important than DNA in that purpose, as the RNA itself is synthesized from DNA during the transcription process [80] which in turn produces proteins in the body by structures call ribosomes [81]. This concludes that both DNA and RNA possess an important role in the drug design field and they are also the key factor for many deadly diseases. Thus, in this context, we have studied the binding properties of nucleic acid (ct DNA, tRNA) and BSA with our complexes (**1**)–(**4**) compared to the parent ligand (H_2L) using absorption and emission studies.

4.1.1. Absorption studies

4.1.1.1. Ct DNA/tRNA binding studies. Electronic absorption titration of the ligand and its complexes (**1**)–(**4**) has been carried out using UV–visible absorption spectra of the tested compounds in the absence and presence of nucleic acid in the range of 200–600 nm. With the incremental addition of ct DNA/tRNA to a fixed concentration of the compounds, the absorption band observed at 350–420 nm decreased with 6–20% hypochromism. This confirms that the compounds undergo interaction with the nucleic acids *via* intercalation mode [82]. This mode of interaction is typically due to the π-π stacking interaction of aromatic chromophore of the ligand with the base pairs of the nucleic acid, which result in conformational alternation on the molecules of DNA [83]. The binding strength of the compounds with nucleic acid has been determined based on the intrinsic binding constant (K_b) using the Wolfe–Shimer Eq. (2) [84,85]:

$$\frac{[\text{Nucleic acid}]}{(\varepsilon_a - \varepsilon_f)} = \frac{[\text{Nucleic acid}]}{(\varepsilon_b - \varepsilon_f)} + \frac{1}{K_b(\varepsilon_b - \varepsilon_f)} \ldots \quad (2)$$

Where [Nucleic acid] is the molar concentration of ct DNA or tRNA, ε_a is the apparent extinction coefficient of the complex bound to nucleic acid (A_{obs}/[compound]), ε_f and ε_b are the extinction coefficients of the free complex and that fully bound to DNA, respectively. The electronic spectral changes upon addition of the nucleic acid to the complexes (**1**)–(**4**) are presented in Fig. 5 and Fig. S6a, ESI† for the ligand. The equilibrium binding constant (K_b) was obtained from the plot of [DNA] or [RNA]/(ε_a - ε_f) *vs* [DNA] or [RNA] (Fig. 5) and dividing slope over the intercept. The intrinsic binding constant (K_b) of the compounds was found to be in the order 10^4 M^{-1} as depicted in Table 3. The K_b values for the complexes are of the order (**4**) > (**3**) > (**1**) > (**2**) > (**H_2L**). This indicates that the binding affinity of complexes is increased than that of the ligand to ~2.5–8.0-fold for ct DNA and 12–24-fold for tRNA. The binding affinities of tRNA to the metal complexes are greater than those of the DNA (4.5–8.9 × 10^4 M^{-1}), which was expected due to striking differences in the 3-dimensional morphology of ct DNA and tRNA. Moreover, in contrast to DNA, the minor groove of RNA helix is wider (shallow minor groove), which is more accessible for specific binders, to form hydrogen bonds to the hydroxyl and phosphate groups with the aromatic chromophore ligand [86]. The binding constant (K_b) values of the compounds are 4.60 (**4**) > 3.40 (**3**) > 2.02 (**1**) > 1.38 (**2**) > 0.58 (**H_2L**) × 10^4 M^{-1} for ct DNA and 8.90 (**4**) > 6.90 (**3**) > 5.40 (**1**) > 4.50 (**2**) > 0.37 (**H_2L**) × 10^4 M^{-1} for tRNA (Table 3), which are similar to

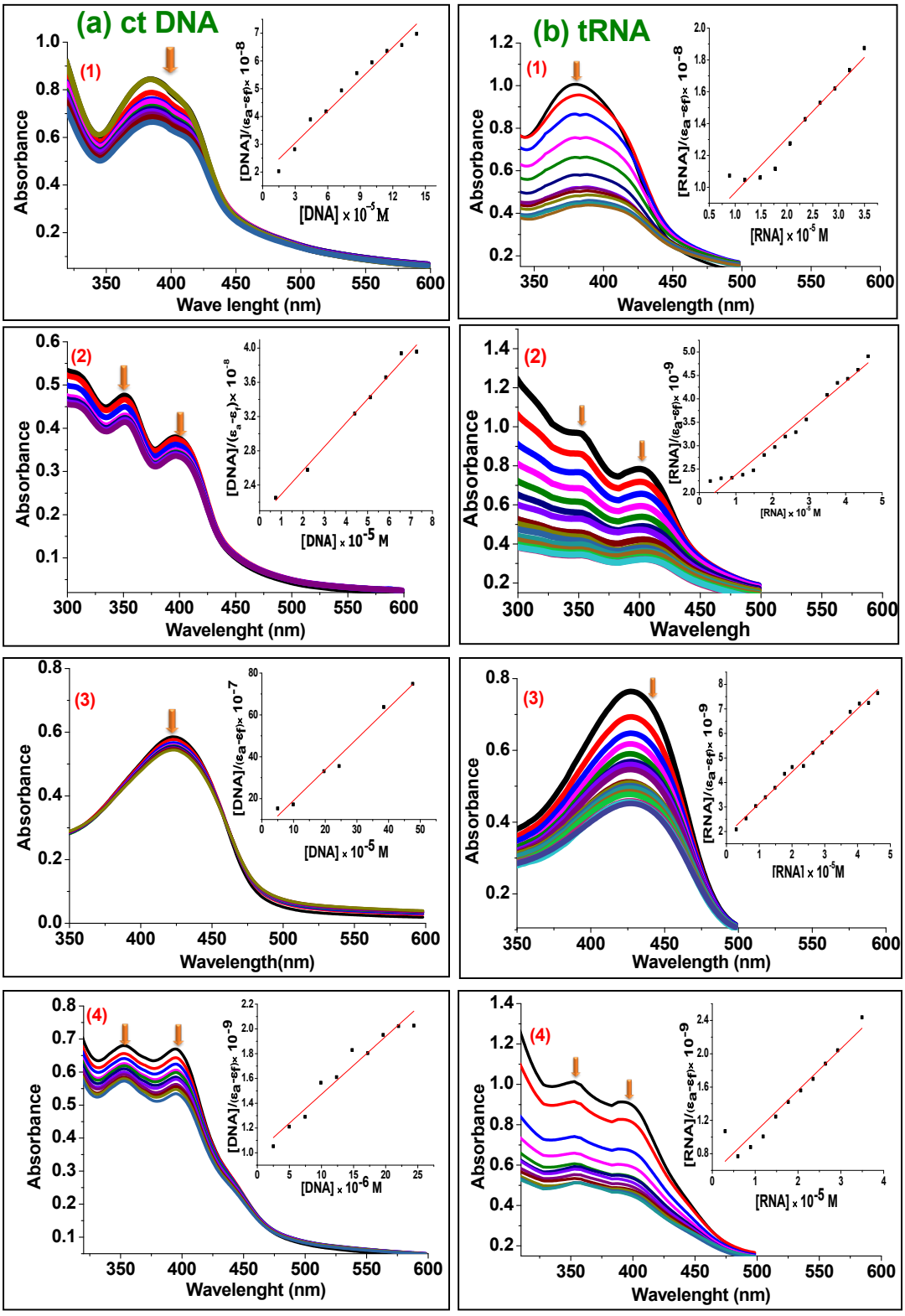

Fig. 5. Electronic spectral changes of the complexes (**1**)–(**4**) in Tris-HCl buffer (pH =7.2) upon addition of different concentrations of **(a)** ctDNA, **(b)** tRNA. Inset: plot of [DNA] or [RNA]/(ε_a - ε_f) *vs* [DNA] or [RNA].

those obtained for related nickel(II) and palladium(II)-PPh_3 base complexes of hydrazone complexes [8,74].

4.1.1.2. Bovine Serum Albumin (BSA) binding studies. Study the interaction of small molecules with bovine serum albumin (BSA) have recently received much attention from researchers in chemistry, biology, and pharmacology due to their significant importance in pharmacology as it consists of 76% similarity with HSA [87]. The electronic absorption study is a very useful tool to evaluate the quenching type (static or dynamic) as well as the structural changes of BSA by the effect of interaction with small molecule drugs [88]. This study has been performed for BSA without and with different

Table 3
Ct DNA and tRNA binding constants (K_b, K_{sv}, K_q and K_{app}) obtained from absorption and fluorescence spectroscopy for the ligand and its complexes.

Compound	Absorption spectroscopy		Emission spectroscopy				
	$(K_b) \times 10^4$		K_{sv} $(M^{-1}) \times 10^3$		K_q $(M^{-1}S^{-1}) \times 10^{11}$		$K_{app} \times 10^5$
	ct DNA	tRNA	ct DNA	tRNA	ct DNA	tRNA	ct DNA
H_2L	0.58	0.37	2.95	2.65	1.34	1.2	2.7
(1)	2.02	5.4	3.76	2.82	1.7	1.28	3.7
(2)	1.38	4.5	−1.97	–	−0.89	–	–
(3)	3.4	6.9	8.4	6.69	3.8	3.04	7.9
(4)	4.6	8.9	12	9.46	5.45	4.3	8

concentrations of the test compounds (ligand and its complexes) in Tris-HCl buffer (pH 7.2) in the range 200–320 nm. The absorption spectra of complexes (**2**)–(**4**) are presented in Fig. 6 (as representative examples), the ligand and complex (**1**) are presented in (Fig. S6b, ESI†) and the binding constant data are depicted in Table 4. It has been observed that increasing the concentration of the compounds results in increasing the absorbance intensity with hyperchromism from 5.30–62.5% for all compounds with blue-shift (4–5 nm) for the complexes. This informs that the interaction between BSA and the test compounds is static and the complexes are in the ground state [89]. These data may also explore that the structural changes have occurred as a result of non-covalent binding mode (electrostatic or *via* hydrogen bonding interaction between the compounds and BSA). In complex (**2**), an isosbestic point (not sharp) was observed at *ca.* 293 nm, which indicated that the interaction between BSA and the complex attained equilibrium [90,91]. The binding strength of the compounds with BSA has been determined using Benesi–Hildebrand Eq. (3) [88]:

$$\frac{(A_\infty - A_o)}{(A_x - A_o)} = \frac{1}{K_b[\text{compound}]} + 1\ldots \quad (3)$$

Where A_o is the absorbance of free BSA, A_x, the absorbance of BSA upon addition of different concentrations of the compounds, and A_∞ is the fully bound BSA with the compounds. The binding constants for the ligand and its complexes can be obtained from the linear relation between $(A_\infty–A_o)/(A_x–A_o)$ against (1/[compound]) (Fig. 6, Fig. S6b, ESI†) and intercept to slope ratio. The obtained binding constants of the compounds are (1.70–4.29) $\times 10^4$ M^{-1} and in the order of (**4**) > (**3**) > (**1**) > (**2**) > (**H_2L**). The same as ctDNA and tRNA, the compounds follow the same order and the complex (**4**) had the highest binding affinity with the protein in a spontaneous fashion.

It is worth noting that the process of dynamic quenching occurs only in the excited state, where the lifetime is extremely short, the quencher (compounds) and fluorophore (BSA) come into contact during the temporary existence of the excited state, and it has no role in the absorption spectrum [92].

4.1.2. *Emission studies*

Fluorescence quenching is considered an important technique to study the binding affinity of the drug and biomolecules (DNA, RNA and proteins). The binding affinity of the synthesized compounds cannot be directly detected by emission spectra, as they don't show any fluorescence in presence of ct DNA or tRNA, hence ethidium bromide (EB) displacement assay has been employed to investigate the binding affinity of ctDNA and tRNA to metal complexes. Ethidium bromide (EB) is the most widely applied fluorophore that strongly intercalates between base pairs of DNA and RNA to flourish a fluorescence that can be measured at 600 nm [93].

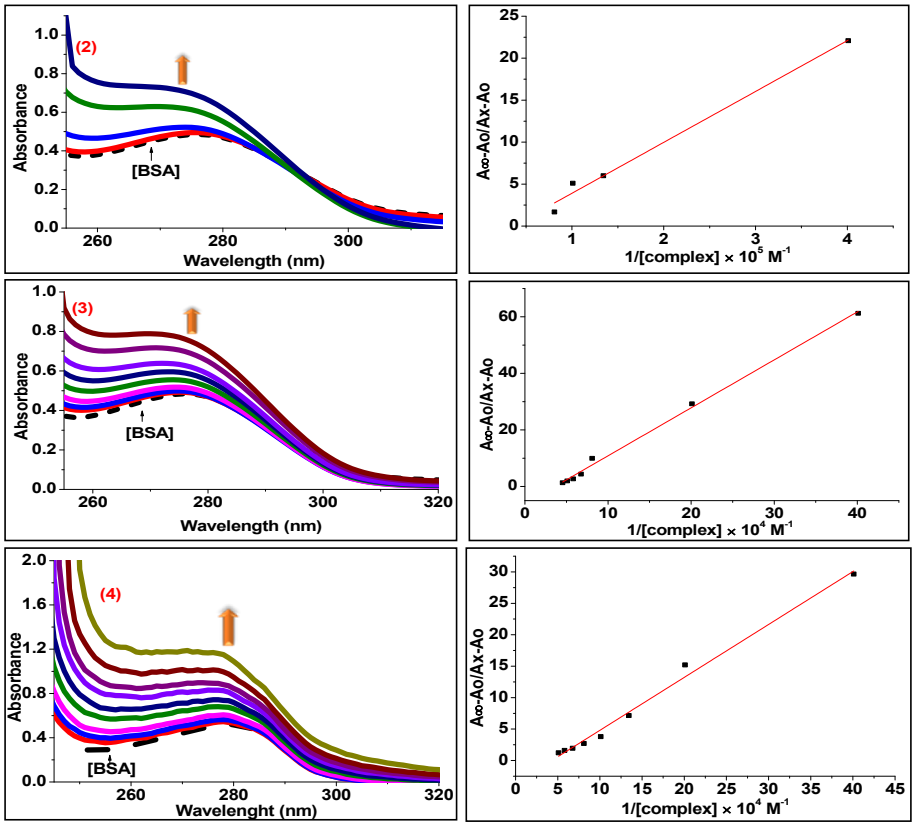

Fig. 6. (Left): Absorption spectra of BSA (15 μM) in absence and presence of increasing amounts complexes (**2**)–(**4**) (0–30 μM) in Tris-HCl buffer pH = 7.2 at 25 °C. Arrow indicates the changes in absorbance upon increasing the compound concentration. (Right): Benesi – Hildebrand linear plot $[(A_\infty\text{-}A_o)/(A_x\text{-}A_o)]$ *versus* 1/[compound] (Right).

Table 4
The BSA binding constants and parameters (K_b, K_{sv}, K_q, K_a, and n) for the ligand and its complexes.

Complex	Absorption spectroscopy	Emission spectroscopy				
		Stern-Volmer		Modified Stern Volmer (MSV)	Scatchard	
	$(K_b) \times 10^4$	K_{sv}	K_q	K_a	K_b	n
H_2L	1.7	–	–	–	–	–
(1)	3.57	1.50×10^4	1.50×10^{12}	1.20×10^4	4.4×10^5	1.35
(2)	3.55	1.00×10^4	1.00×10^{12}	1.14×10^4	5.1×10^4	1.3
(3)	3.6	1.60×10^4	1.60×10^{12}	1.19×10^4	7.1×10^4	1.16
(4)	4.29	–	–	1.50×10^4	1.1×10^6	1.37

4.1.2.1. Ct DNA and tRNA binding studies.. If the test compound can displace ethidium bromide from ctDNA/tRNA-EB adduct, the fluorescence intensity will be quenched (due to the formation of a non-fluorescent complex), and the interaction between the small molecule and the nucleic acid will be intercalation [94,95]. On the other hand, if the complex failed to displace EB from nucleic acid-EB, the surface or groove binding may take place. In the present study, while adding increasing amounts of the complexes to nucleic acid-ethidium bromide (NA-EB) adduct, the fluorescence intensity at 580 nm is reduced for the **H_2L** and its (**1**, **3**, **4**) complexes (Fig. 7 and H_2L (Fig. S6c). Conversely, the palladium complex (**2**) showed a different mode of interaction, where the fluorescence intensity is enhanced upon addition of the complex (Fig. 7), this indicates that this complex (**2**) interacted with ctDNA-EB adduct *via* another way rather than intercalation (interact *via* non-competitive inhibition) and a negative binding constant was obtained [96–98]. Furthermore, in the case of yeast tRNA (Fig. 7), the emission intensity is decreased at the beginning within the concentrations (5–25 μM) with 17% hypochromism and bathochromic shift of 4 nm, then the enhancement takes place with the concentrations (30–75 μM) with 10% hyperchromism and bathochromic shift 7 nm, which also confirms that interaction of tRNA with complex (**2**) occurs differently (intercalation along with surface binding)[98], for the differential structure of DNA and RNA [99].

The quenching efficiency can be measured from Stern-Volmer Eq. (4) [46]:

$$F^o/F = 1 + K_{sv}[Q], \quad (4)$$

Where F^o and F stand for the fluorescence intensities before and after the addition of quencher, respectively, K_{sv} is Stern-Volmer rate constant, and [Q] is the concentration of the quencher. K_{sv} is obtained from the slope of the linear relation between F^o/F and [Q] and the K_{sv} values were presented in Table 3.

The dynamic or collision quenching constant (K_q) can be calculated from K_{sv} using the Eq. (5):

$$K_{sv} = K_q \tau_o, \quad (5)$$

Where τ_o is the lifetime of the fluorophore in absence of the quencher, which is often approximate at 10^{-8} s [100]. It was found that the calculated biomolecular rate constant (K_{sv}, Table 3) is higher than (2.0×10^{10} $M^{-1}S^{-1}$), the maximum collisional quenching of different types of biopolymer quencher, which confirm the results obtained from absorption spectra, the quenching takes place through NA-complex formation [82].

Furthermore, the apparent binding constant (K_{app}) can be evaluated using the Eq. (6).

$$K_{EB}[EB] = K_{app}[Complex]_{50\%} \quad (6)$$

Where K_{EB} is 1.0×10^7 and [EB] = 5 μM and $[Complex]_{50\%}$ is the complex concentration at a 50% reduction of the fluorescence intensity. It has been found that all binding constant values (K_{sv}, K_q, and K_{app}) follow the order: (**4**) > (**3**) > (**1**) > (**H_2L**) as shown in Table 3. The complex (**2**) is not in order, as the enhancement is observed in Fig. 5b. These results reveal that, among all compounds, the Ru(II) complex (**4**) possesses the strongest affinity to ctDNA and tRNA. By comparing with some Schiff base metal complexes of triphenylphosphine [26,48,54,74,95], the reported binding constants are in the order 10^3–10^4 M^{-1} range which is similar or lower than those obtained in the current study.

4.1.2.2. BSA binding studies. The binding properties of BSA with the synthesized compounds have been also studied using fluorescence spectroscopy to confirm whether the BSA-complex formation follows a static or a dynamic quenching mechanism. The emission spectrum of BSA shows its characteristic peak at ~340 nm (excited at 290 nm) that is associated with the existence of tryptophan residues (Trp134 and Trp 213). Trp 134 is located on the surface of the protein, while Trp213 residue present within a hydrophobic binding pocket of the molecules. Both residues have an intrinsic fluorescence [101,102]. The successive addition of the compounds to BSA in buffer solution results in quenching in fluorescence intensity in the complexes (**1**)–(**4**). This quenching is usually assigned to static quenching mechanism as the changes occur in BSA secondary structure as a result of binding to the compounds, and this indicates that the formation of a ground state new complex between BSA and metal complexes rather than dynamic collision [103]. Conversely, in the addition of different amounts of H_2L to BSA solution, the intrinsic fluorescence of protein is enhanced at 450 and 485 nm, where their interaction may occur in different a different mechanism [104]. Emission spectra of the ligand (H_2L) and complexes (**1**)–(**4**) are shown in (Fig. S6d, ESI†).

The Stern-Volumer (K_{sv}) and quenching rate (K_q) constants were obtained from Stern-Volumer Eqs. (4) and (5), respectively. Both values (K_{sv} and K_q) were obtained from the plot of F^o/F *versus* [Q] for complexes (**1**)–(**3**), but not for H_2L and complex (**4**) due to the negative slope and nonlinearity, respectively. So, the quenching process was further analyzed using the modified Stern-Volmer Eq. (7) [105] below for the complexes (**1**)–(**4**) (Fig. 8).

$$\frac{F^o}{(F^o - F)} = \frac{1}{f_a K_a [Q]} + \frac{1}{f_a} \quad (7)$$

Where F^o and F were mentioned above, f_a is the fractional accessible protein fluorophore, [Q] is the molar concentration of the quencher and K_a is the effective quenching constant for the accessible fluorophore, which is similar to the association binding constants for the quencher acceptor system. It can be obtained from the intercept ($1/f_a$) to slope ($1/f_aK_a$) ratio from straight line obtained after plotting F^o/F^o-F against $1/[Q]$, as shown in Fig. 8. This linear relationship confirms a static quenching mechanism has taken place for the interaction of complexes with BSA. The quenching constant K_a for the complexes follow the following order (Table 4):

Additionally, the binding constant (K_b) and the number of binding sites (n) in static quenching can be calculated using Scatchard Eq. (8) [106,107] for static quenching,

$$Log_{10}[(F^o - F)/F] = Log_{10} K_b + n Log_{10}[Q] \quad (8)$$

Where F^o and F are defined the same as above, the values of K_b and n values are given in Table 4 which obtained from the inverse logarithm of the intercept and the slope, respectively from the interpolations of Log [(F^o – F)/F] *versus* Log[Q]. The binding affinity is found in the order (**4**) > (**1**) > (**3**) ~ (**2**) to show that the complex (**4**) still has the highest binding constant with nucleic acids and protein as shown in Table 4. For

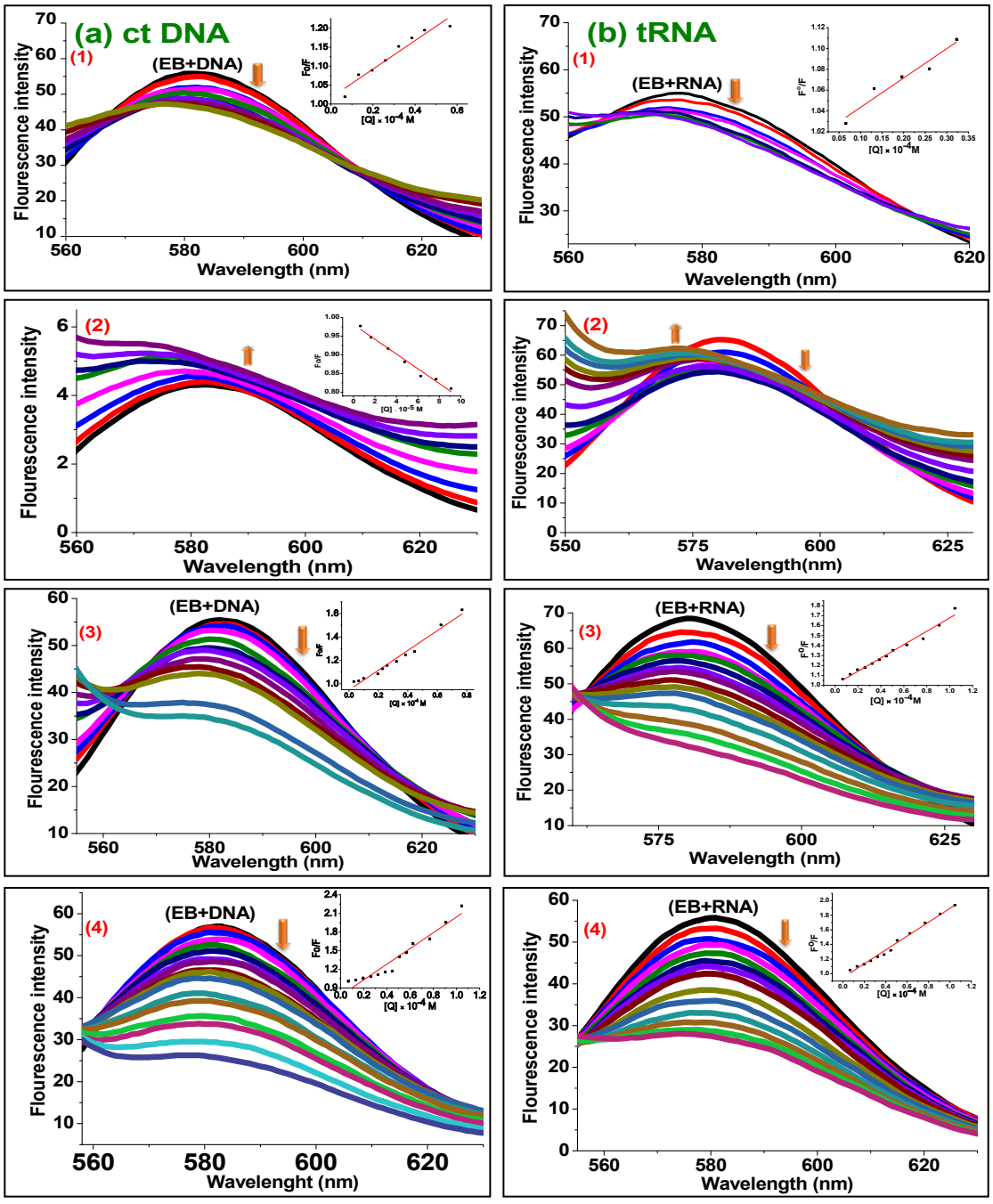

Fig. 7. Fluorescence quenching curves of EB- bound; (a) ct DNA and (b) tRNA in presence of complexes (**1**)–(**4**);[EB] = 5 μM, [DNA] = [RNA] = 80 μM, [complex] = 0–140 μM. Inset: plot of F^o/F *vs.* [Q].

all complexes, the number of the binding sites (*n*) on BSA was in the range (1.16–1.37) as shown in Table 4 and Fig. S6e. which indicates the existence of a single available binding site for the complexes [108].

4.2. Antioxidant activity

The antioxidant activity of the ligand and its complexes has been evaluated using DPPH radical assay. In DPPH, scavenging activity, the antioxidant scavenges the free radical by donation of hydrogen, which can be observed visually, as the color becomes lighter (purple to yellow). The DPPH assay is one of the most useful methods used for evaluating the antioxidant activity of the compounds depending on the electron/proton donation capacity. This assay can be affected by numerous factors, such as the concentration of hydrogen, metal ions, amount of solvent. In this method, the chromogen free radical ($DPPH^{\bullet}$) reacts with the test compounds (antioxidant). Due to accepting a proton or electron donation, the purple color of the chromogen changes into yellow in the solution, and this change was followed spectrophotometrically at 517 nm. The reaction can be simply presented as $DPPH^{\bullet} + HA \rightarrow DPPH\text{-}H + A^{\bullet}$. The reduction of color depends on the concentration of the compounds which led to the enhancement of radical inhibition. As shown in Table 5. The DPPH scavenging activity of the complexes is higher than that of the free ligand indicating that the chelation to the metal ion enhances the activity, and the radical scavenging activity of the test compounds as well as ascorbic acid is concentration-dependent as shown in complex (**4**) (Fig. 9 as an example), and Fig. S7, ESI†). The higher antioxidant activity results were taken as a lower value of IC_{50} of order (Table 5) which of the order: AA >**4** > **3** > **1** > **2** > H_2L. The

(4 3 1 > (2)

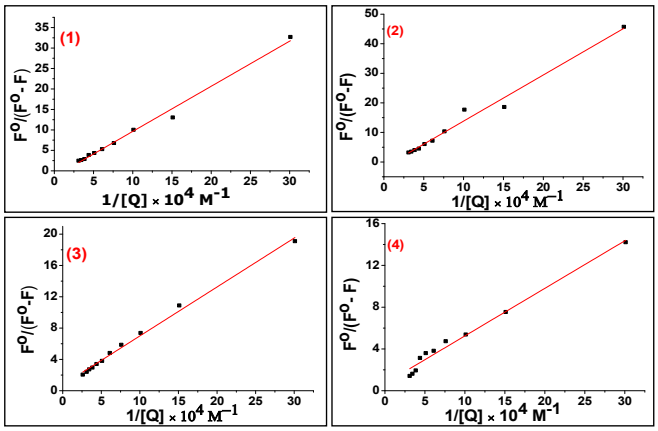

Fig. 8. Modified Stern –Volmer plot for the quenching of BSA fluorescence complexes (**1**)–(**4**).

Table 5
Antioxidant parameters in DPPH scavenging activity data of the ligand and its complexes.

Compound	IC_{50}	EC_{50} [a]	ARP [a]	Stoichiometry [a]	No of reduced DPPH [a]
H_2L	408	4.08	0.25	8.16	0.12
(1)	235	2.35	0.43	4.7	0.21
(2)	270	2.7	0.37	5.4	0.18
(3)	91	0.91	1.09	1.82	0.55
(4)	55	0.55	1.82	1.1	0.91
Ascorbic acid	43	0.43	2.32	0.86	1.16

[a] EC_{50} (μmol of antioxidant/μmol DPPH), ARP = $1/EC_{50}$, stoichiometry = 2 × EC_{50}, no. of reduced DPPH = 1/stoichiometry.

complex (**4**) exhibited the highest scavenging activity among all compounds (IC_{50} = 55 μM), which is similar to that reported for potent antioxidants of ruthenium(II) and vanadium(IV) complexes containing similar O,N,S-donor ligand [48]. The other antioxidant parameters; EC_{50}, ARP, stoichiometry and number of reduced DPPH• radicals have been calculated, and we found that the lower IC_{50} and EC_{50} values, the greater ARP values [48].

4.3. *In vitro cytotoxic activity (MTT assay)*

The interesting results collected from ct DNA, tRNA, BSA binding affinity, and antioxidant properties of the synthesized compounds have prompted us to evaluate their anticancer activity against human cancer cell lines; Colorectal carcinoma Colon cancer (HCT116), Hepatocellular carcinoma (HepG2), and mammary gland breast cancer (MCF7) along with the human lung fibroblast (WI38) as a non-tumor cell line and compared to *cis*-platin as positive control by MTT assay. The cell viability percentage was plotted against the concentration of the compounds after 24 and 48 h of treatment (Fig. S8, ESI†). As shown in these figures, the cell viability decreased in a concentration-dependent manner and incubation period as well as the type of cancer cell [109,110]. The data are presented based on IC_{50} (the half-maximum inhibitory concentration) and selectivity index (SI) = IC_{50} of normal cell/IC_{50} of cancer cell) [111] as shown in (Figs. 10 and 11, and Table S3, S4), and respectively. The IC_{50} values showed the higher activity of metal complexes in a 48 h period, this may be attributed to the high kinetic stability of the complexes in culture media [112]. It has been shown that the complex (**4**) showed the lowest IC_{50} (highest cytotoxic activity) on HepG2 (26.14 ± 2.0 μM) and HCT116 (22.02 ± 1.9 μM) and the highest selectivity index, 3.75 and 4.45, respectively. On the other hand, nickel(II) complex (**1**) showed the lowest IC_{50} on MCF7 (14.35 ± 1.4 μM) highest selectivity index 5.59. The cytotoxic activity of the compounds was found to follow the order on the basis of IC_{50}:

HepG2: (**4**) > (**3**) > (**1**) > (**2**) > (**H_2L**)
HCT116: (**4**) > (**3**) > (**1**) > (**H_2L**) > (**2**)
MCF7: (**1**) > (**4**) > (**3**) > (**H_2L**) ≈ (**2**)

In comparing ruthenium(II) complexes with platinum(II) complexes, it is known that ruthenium complexes have several characteristic properties over the platinum complexes such as, octahedral geometry, which induces the structure diversity as compared to square planar platinum(II) complexes, multiple accessible oxidation states (+II to +IV) under physiological conditions, and kinetic lability of ruthenium(II) species which facilitate the ligand exchange reaction and leads to more rapid interaction with biological targets molecules [113,114]. In addition to the concentration of the tested compound and the incubation period, the anticancer activity may also be affected by the structure-activity relationship [115]. For instance, among the three square planar complexes (**1**)–(**3**), the Pt(II) complex exhibited a better cytotoxic activity (in terms of IC_{50} values) towards HePG2 (28.94 ± 2.4 μM) and HCT116 (31.11 ± 2.8 μM) after 48 h of treatment, while it showed moderate activity against MCF7 (44.76 ± 3.4 μM), but the Ni(II) complex (**1**) exhibited a high selectivity index to all tested cancer cell lines (1.59–3.03), and presented a safely profile towards the normal cell line (WI38, IC_{50} = 80.30 ± 4.2 μM). This may attribute to the structure diversity of cationic Pt(II) complex (**3**), where, the ligand acts as a mono-negative bidentate rather than bi-negative tridentate in the rest of the complexes. Among all the compounds, Ru(II) and Ni(II) complexes displayed interesting activity towards cancer cells as their selectivity indices (3.46–5.59) are higher than 3.0, comparable to that of cisplatin

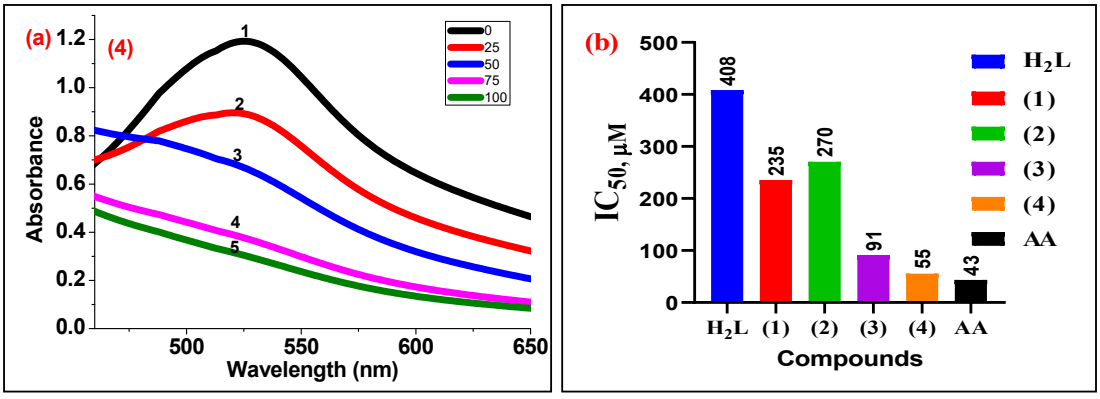

Fig. 9. (a) Changes in UV–Vis spectrum of DPPH (100 μM) in the presence of complex (**4**) (25–100 μM) after 30 min incubation in DMSO at room temperature, (b) DPPH scavenging activity of the compounds on the bases of IC_{50}.

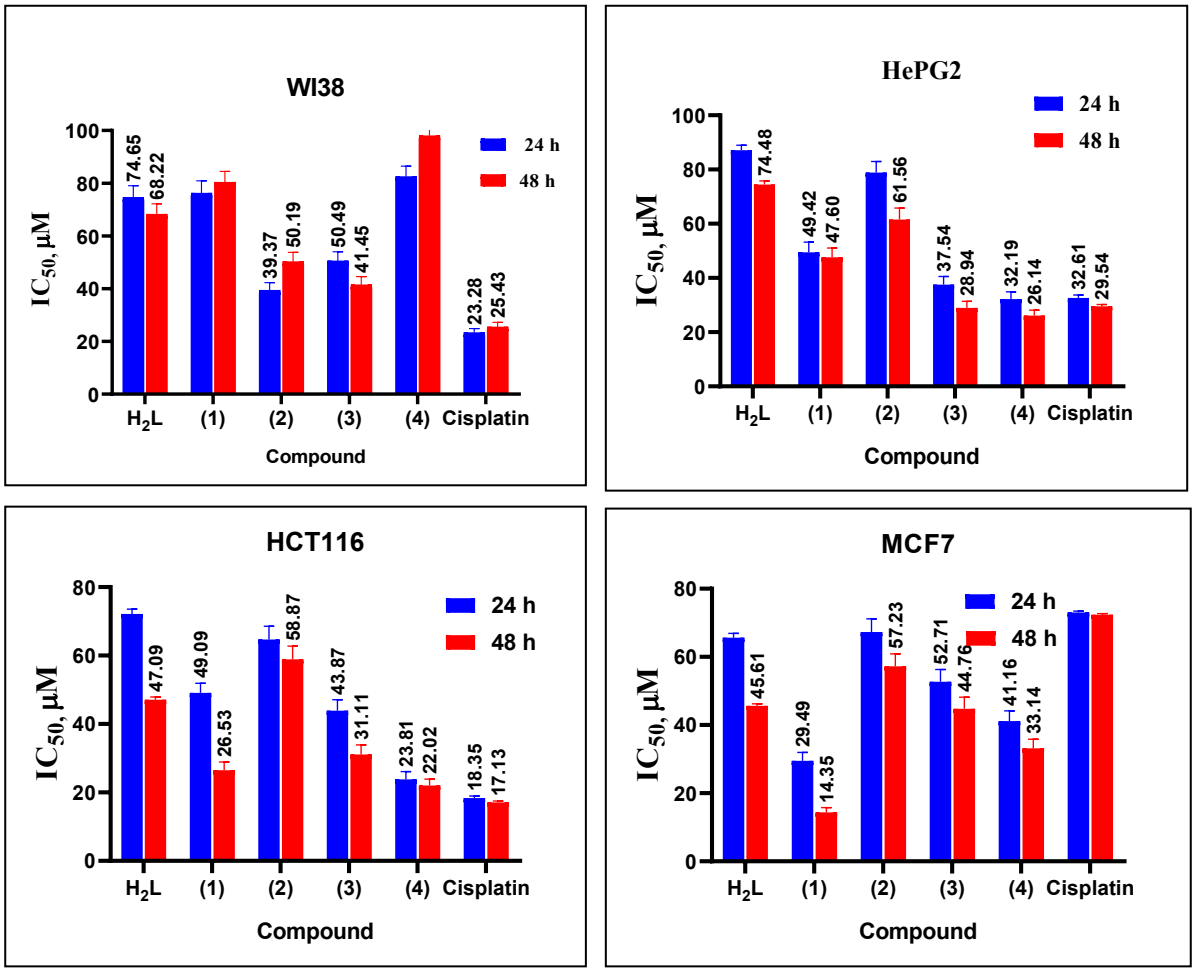

Fig. 10. Cytotoxicity (IC_{50} values) of the (Ligand (H_2L), complexes (**1**)–(**4**) and cisplatin) at 24 and 48 h against WI38, HepG2, HCT116, and MCF7 cell lines.

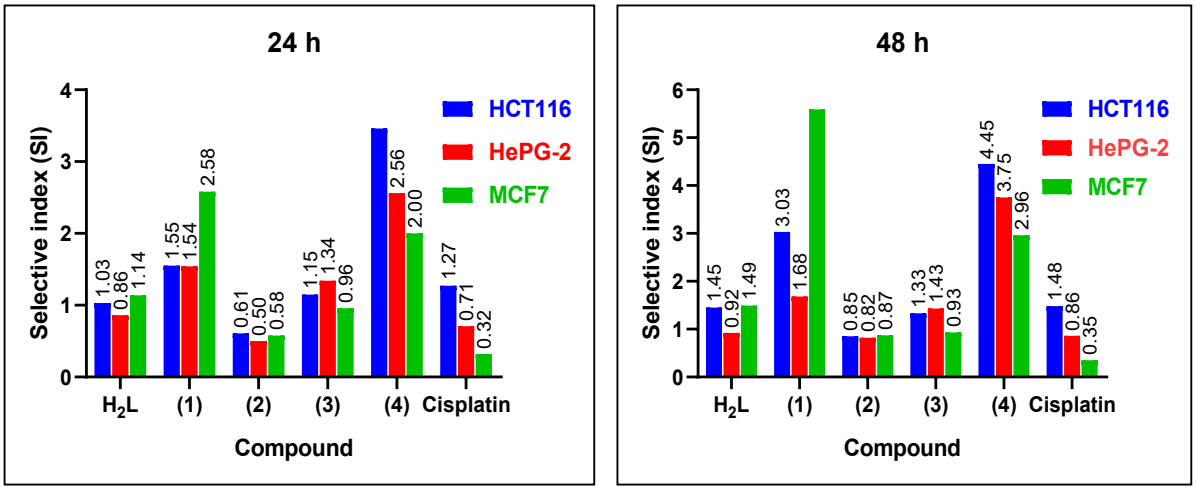

Fig. 11. Selective indices of the ligand and complexes towards cancer cell lines at 24 and 48 h.

(< 1.5). This provide a high selectivity towards particular human cancer cell lines [116]. It is worth noting that the selectivity of the compounds towards cancer cells can be determined by the selectivity index (SI), which becomes an essential prerequisite to estimate the capability of the test compound to kill the cancerous cells without harming the healthy one [117]. The higher the SI, the higher selectivity of the compounds. It has been reported that the compounds which have SI ≥ 3 are considered highly selective towards a specific cell line, so it becomes a curial requirement for the development of a chemotherapeutic agent with good selectivity towards cancer cells [118,119].

The complexes provide comparable cytotoxic levels with some other reported complexes for the selected tumor cell lines. It has been reported that a series of Ni(II) triphenylphosphine complexes with thioamide derivatives [120] or aroylhydrazone [95] has shown IC_{50} of 20–40 and

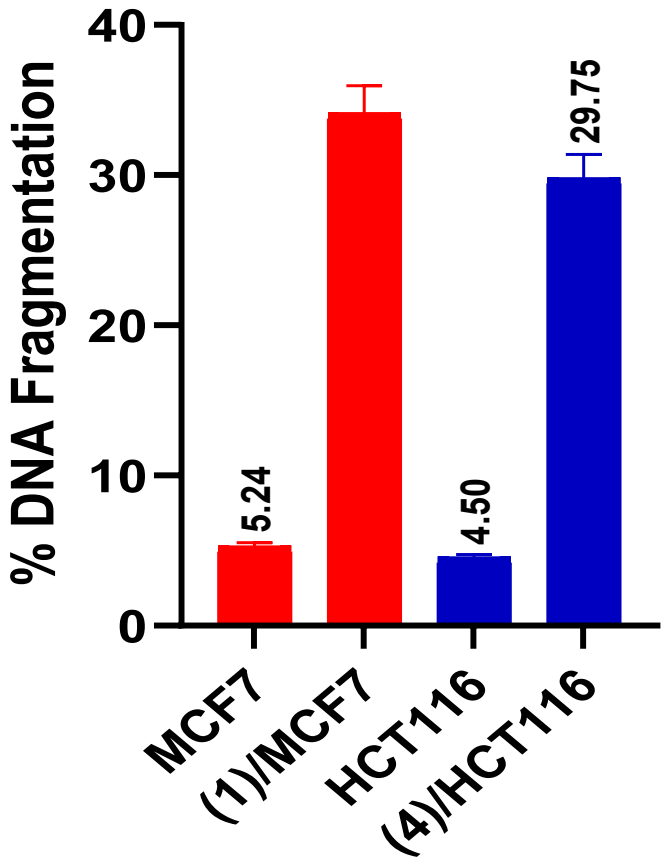

Fig. 12. DNA fragmentation using DPA assay for complex (**1**) on MCF7, and complex (**4**) on HCT116, MCF7, and HCT116 cell lines as control.

32.6 μM, respectively against MCF7 cell line and they showed higher toxicity to cancer cells than *cis*-platin, which support the Ni(II) complex possesses the potential to act as effective metal-based anticancer drugs.

4.4. Apoptotic activity

Apoptosis and necrosis are two major forms of cell death [121,122] Apoptosis (or programmed cell death) plays an essential role in regulating cell death by controlling the number and size of the cells. Necrosis (sudden cell death), usually causes spillage of cell contents into surrounding tissues, consequently, cell damage takes place. Inappropriate regulation of apoptosis can result in various forms of diseases including cancer [123]. To distinguish between apoptotic and necrotic cell death, cell cycle assays by Annexin has been carried out by following cytometric technique. Based on ct DNA/tRNA and BSA interaction studies, along with antioxidant and cytotoxic properties of the synthesized compounds, complexes (**1**) and (**4**) exhibited better activities compared to their parent ligand and other complexes. So, both complexes were further selected for investigating their efficacy in cell death in MCF7 and HCT116 cells, respectively. The induction of apoptosis was studied by the colorimetric diphenylamine (DPA) assay and flow cytometric analysis of DNA contents.

4.4.1. DNA fragmentation

The DNA fragmentation was quantitatively determined using the colorimetric diphenylamine assay (DPA) [124]. The complexes (**1**) and (**4**) were selected for DNA fragmentation analysis. The fragmentation percentage data were presented with respect to the control (untreated cells) in Fig. 12 and Table S5. The breast cancer cells (MCF7) were treated with complex (**1**) at $IC_{50} = 14.35 \pm 1.4$ μM, it was found that the DNA fragmentation percent was 34.09 ± 1.86% (control, 5.24 ± 0.29%). In the case of treatment of colon cancer cells (HCT116) with complex (**4**) at $IC_{50} = 22.02 \pm 1.9$ μM, the fragmentation percent was 29.75 ± 1.62 (control, 4.5 ± 0.25). This concludes that the fragmentation percent of each complex compared to its selected cell lines increased *ca.* 6.5-fold compared to control cells for 48 h. These findings may suggest that complexes promote cell death *via* DNA damage [125].

4.4.2. Apoptosis analysis by flow cytometry

Flow cytometry is considered one of the most effective methods to analyze cell death and evaluate the therapeutic efficacies of anti-cancer drugs [126]. Most of the anticancer agents inhibit cancer cell proliferation by induction of apoptosis in tumor cells [127]. To determine the cellular DNA content and the growth inhibition mechanism on tumor cells, the flow cytometry technique has been employed.

4.4.2.1. Cell apoptosis. The apoptotic cell death in MCF7 and HCT116 was investigated by flow cytometry using co-staining of annexin-V FITC and (PI). Generally, the cells are distributed in four different quadrants (Q1-Q4) as shown in Fig. S9, ESI†, Q1 (live cells, lower left quadrant), Q2 (early apoptosis, lower right quadrant), Q3 (late apoptosis, upper right quadrant) and Q4 (necrosis, upper left quadrant). The MCF7 cells were treated with complex (**1**) at IC_{50} concentration for 48 h. In control (untreated MCF7 cells), the living cell % was 98.15% and apoptotic % was 1.03%. On the treatment of MCF7 cells with the complex (**1**), the apoptotic percent increased to 24.58% (2.33% early and 22.25% late apoptosis), *i.e.* 23.86-fold (control, 1.03%), this indicates that the complex can induce cell death *via* apoptosis. It has been also noted that

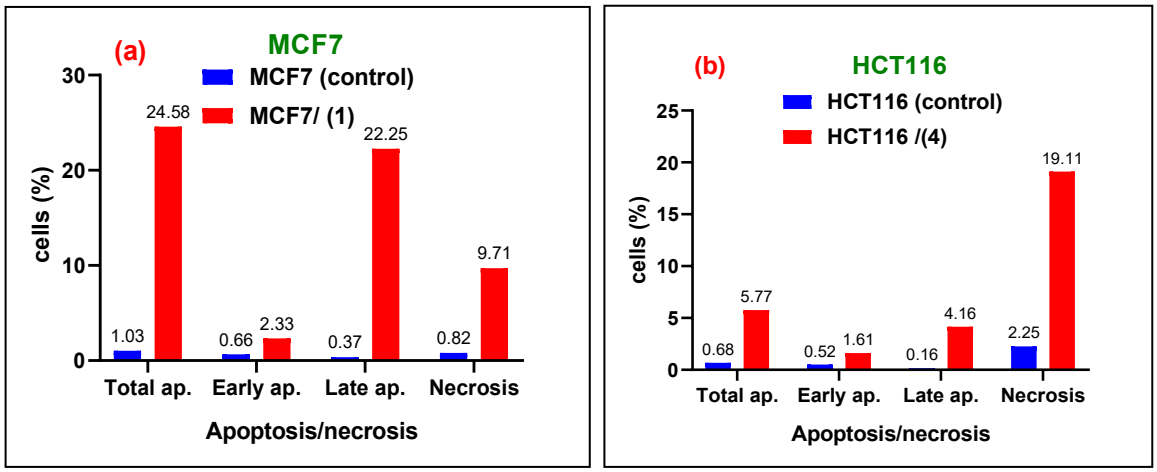

Fig. 13. Apoptosis/necrosis cell percentages of: (a) MCF7 with complex (**1**), (b) HCT116 with complex (**4**) after 48 h incubation period at IC_{50} values.

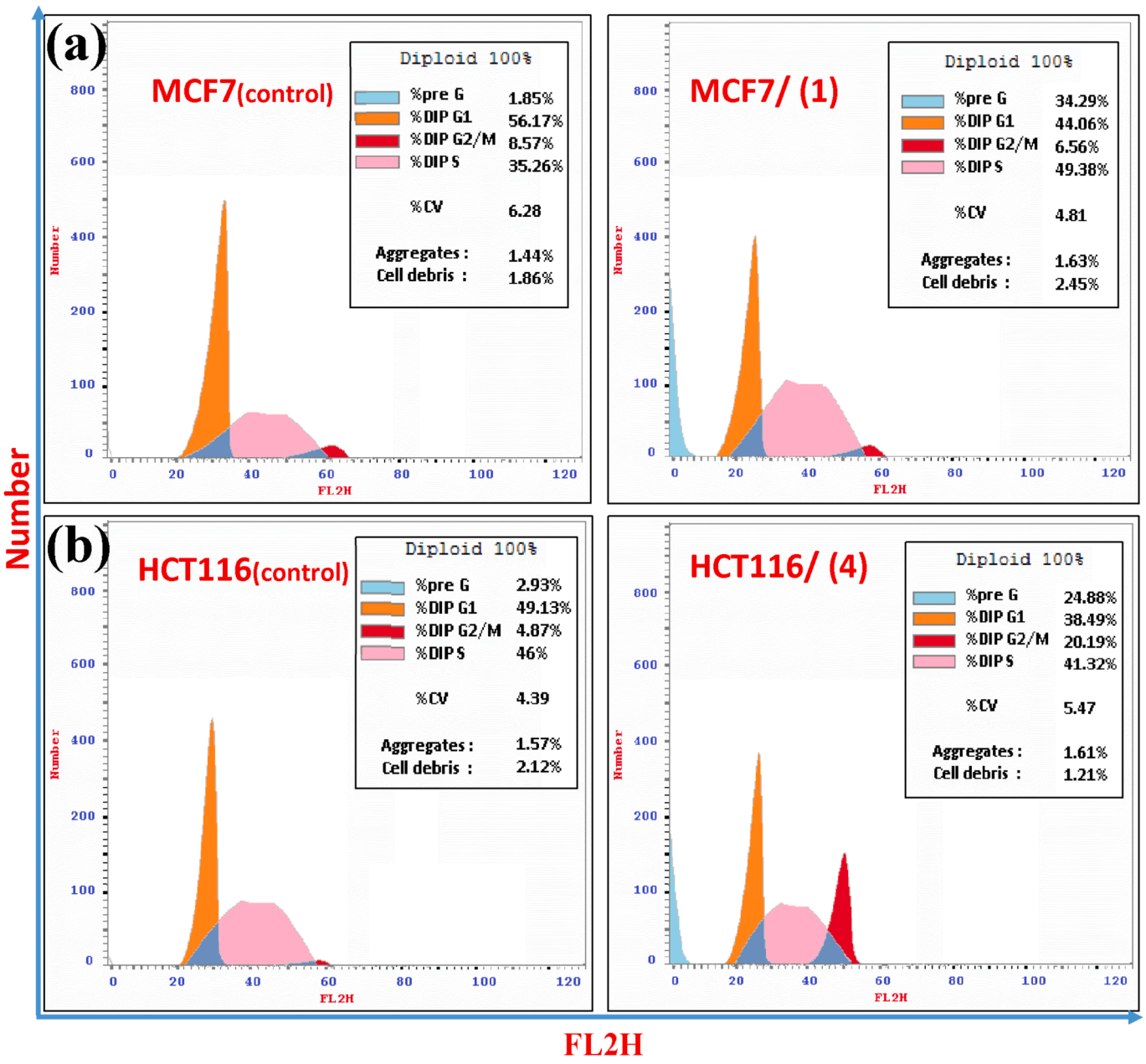

Fig. 14. Percentage of cell populations among cell phases in: (a) untreated (control) and treated cells MCF7 with complex (**1**), (b) untreated (control) and treated HCT116 with complex (**4**) at IC_{50} concentrations for 48 h.

the number of cells in Q4 was increased to 9.71 (control, 0.82%) demonstrated that the cell death mode can, to a slight extent, takes place *via* necrosis. While, the treatment of HCT116 cells with complex (**4**) at IC_{50} concentration for 48 h, the apoptosis percent increased to 5.77% (1.61% early and 4.16% late apoptosis), *i.e.* increased 8.49-fold compared to untreated cells (0.68%), which indicates that the cells may be undergoing apoptosis [128]. It has been also observed that the HCT116 cells increased in necrosis quadrant to 19.11%, by 8.49-fold compared to untreated cells (2.25%), and this result following early reports [129] which demonstrated that Ru(II) complexes can majorly induce cell death through necrosis. Apoptotic cell % is shown in Fig. 13 and (Fig. S9 and Table S6, ESI†).

4.4.2.2. Cell cycle analysis. Based on the inhibitory effect on cell proliferation, the effect of complex (**1**) on the cell cycle of MCF7 cells was evaluated. The analysis of the cell cycle phases was carried out by flow cytometry at IC_{50} concentration for 48 h. Cell cycle phase distribution consists of some phases such as quiescent (G0), interphase (gap1 (G1), synthesis (S), and gap2 (G2)), and mitotic phase (M) [130]. During the cell dividing progression, the cells undergo a transition through (G1) → (S) → (G2) → (M) phases to synthesize DNA, cell division followed by mitosis process. However, if the cells enter the inactive phase (G0 or Pre-G1 phase), this means that the cells enter a resting state (quiescent), where there is no dividing, no proliferation [126].

The effect of complexes (**1**) and (**4**) have been studied on the cell cycle of MCF7 and HCT116 cells, respectively. Complex (**1**) exhibited a significant increase at the pre-G1 phase (~32.44% *versus* untreated cells) (Fig. 14, Fig. S10 and Table S7). Earlier reports indicated that disruption of the pre-G1 phase in the cell cycle might be one of the reasons for apoptosis [131]. The MCF7 cells were arrested in the S phase, since there is an increase in the number of cells by ~14.12% (49.38%, control 35.26%), but an insignificant change (~2.01%) was found at the G2/M phase. This observation along with the DNA fragmentation studies may suggest that the nickel(II) complex (**1**) can stop the MCF7

proliferation by induction of apoptotic cell death. On the other hand, on the treatment of the HCT116 cells with complex (**4**), there was a decrease in the number of cells in G1 phase (38.49%, control 49.13) and S phase (41.32, control 46%) as shown in Fig. 14. However, the number of cells increased in the G2/M phase (20.19, control 4.87%) which means cell cycle arrest at the G2/M phase. That increased in G2/M leads to the accumulation of the cells in this stage indicating the inhibition of HCT116 cells from replication again and this may be due to the strong interaction between the complex (**4**) and the DNA that was previously confirmed by ct DNA binding assay. From the former data, we observed that the complex (**4**) can interact with the cellular protein, as observed from BSA binding affinity, along with strong interaction with nucleic acids which may break the DNA and make unpacked DNA rather than fragmentation, which prevent cancer replication and arrest the cell cycle at G2/M. Moreover, the HCT116 cells treated with ruthenium(II) complex have increased the pre-G1 population which may appear from loosely packed DNA that happened and resulted in a high increase in cell percentage at necrotic quadrant, when analyzed by annexin assay, revealed the induction of necrotic cell death.

Finally, our data revealed the apoptotic cell death of the MCF7 cells treated with complex (**1**) was confirmed by high DNA fragmentation percentage and the good binding affinity with biomolecules (DNA, RNA, and BSA). When complex (**1**) made strong binding with nucleic acid resulting DNA damage and hence the S phase in the cell cycle was arrested, as increased its percentage, and the pre-G1 phase has appeared with high percentage as a result of apoptotic cell death. The MCF7 apoptotic cell death was also confirmed by the annexin V/PI stain, after treated with complex (**1**), with an increase in the total apoptosis % 23.86-fold than control. Cancer cells induced high reactive oxygen species (ROS) as increased metabolism due to increased proliferation rate [132]. The antioxidant potency of the complex (**1**) can scavenge the elevated ROS and inhibited the cancer cell replication and that increased the safety of that complex on healthy cells which is confirmed by the high SI and good cytotoxicity results.

On the other hand, the treatment with complex (**4**) induced an anti-proliferative effect against HCT116 cells *via* making intercalation and surface binding with DNA strands which can unpack the two strands leading to replication inhibition which confirmed by cell cycle arrest at the G2/M phase. Also, the necrotic cell death that appears in annexin V/PI stain data may be attributed to high binding affinity with biomolecules, which can make irreversible binding, and results in the sudden death of the cancer cells (necrotic cell death). However, the DNA fragmentation data of the complex (**4**) may due to the intercalation with DNA that led to unpacked strands rather than truly fragmentation because DNA fragmentation didn't contribute to necrotic cell death. One of the probable hypotheses of the appearance of the pre-G1 phase is the accumulation of dead cells that are affected by the complex (**4**) treatment through necrotic death [133,134]. The accumulated dead cells were due to sudden unpacked DNA strands and they may reduce the fluorescence intensity of the G1 population during cell cycle analysis leading to the appearance of the pre-G1 phase [135,136] Concurrently, the high antioxidant activity of complex (**4**) has increased its safety on healthy cells confirmed with high SI and cytotoxicity values.

5. Conclusions

Synthesis and characterization of new series of Ni(II) (**1**), Pd(II) (**2**), Pt(II) (**3**), and Ru(II) (**4**) complexes bearing 2,4-dihydroxybenzaldehdye-*S*-methyldithiocarbazate (H_2L) and PPh_3 ligands have been described. In complexes; (**1**), (**2**), and (**4**), the ligand coordinates to the metal center in a di-basic tridentate (ONS) manner, while in complex (**3**) coordinates in a mono-basic bidentate (NS) manner. The binding properties of the ligand and complexes with ct DNA, tRNA and BSA were evaluated by UV–Vis and fluorescence spectroscopies revealing the intercalation binding mode for most of complexes. The antioxidant properties of all compounds were investigated using DPPH radical scavenging activity and showed that the complexes have better antioxidant activity compared to the parent ligand. Anticancer activity against four human cell lines has been demonstrated, indicating that all complexes are toxic to cancer cell lines and safe towards the normal one. Finally, complexes (**1**) and (**4**) were selected for DNA fragmentation, apoptotic activity and cell cycle analysis. Our data revealed, complex (**1**) induced apoptotic cell death of the MCF7 cells by fragmentation of the DNA after binding with it, increased pre-G1 phase and arrested the cell cycle at S phase. Also, complex (**1**) has antioxidant activity that helped in scavenging the excess ROS and preventing healthy cell damage along with inhibiting the cancer cell replication. For complex (**4**), it exhibited a good anti-proliferative effect against HCT116 cells that arrested at the G2/M phase. Necrosis induction has also occurred, that may be due to the intercalation and surface binding with DNA strands which can unpack the two strands leading to sudden cell death. Also, the increased safety of the complex (**4**) on the healthy cells was confirmed by its potent antioxidant activity and elevated SI values.

Declaration of Competing Interest

The authors declare that they have no known competing financial interests or personal relationships that could have appeared to influence the work reported in this paper.

Acknowledgments

Authors acknowledge support from the Ministry of Higher Education of Egypt for CIQAP (CP3-016-MAN) project research equipment funds. Special thanks go to Prof. Alessandro Caselli, Prof. of Inorganic Chemistry, *Dipartimento di Chimica*, Università degli Studi di Milano, Milano, Italy, for giving us the opportunity to carry out the X-ray analysis and Mass spectra of complexes.

Appendix A. Supplementary data

Supplementary data to this article can be found online at https://doi.org/10.1016/j.jinorgbio.2021.111549.

References

[1] C.-P. Tan, Y.-Y. Lu, L.-N. Ji, Z.-W. Mao, Metallomics insights into the programmed cell death induced by metal-based anticancer compounds, Metallomics 6 (2014) 978–995, https://doi.org/10.1039/c3mt00225j.
[2] E.R. Jamieson, S.J. Lippard, Structure, recognition, and processing of cisplatin–DNA adducts, Chem. Rev. 99 (1999) 2467–2498, https://doi.org/10.1021/cr980421n.
[3] N.J. Wheate, S. Walker, G.E. Craig, R. Oun, The status of platinum anticancer drugs in the clinic and in clinical trials, Dalton Trans. 39 (2010) 8113–8127, https://doi.org/10.1039/C0DT00292E.
[4] Z. Guo, P.J. Sadler, Metals in medicine, Angew. Chem. Int. Ed. Eng. 38 (1999) 1512–1531, https://doi.org/10.1002/(SICI)1521-3773(19990601)38:11<1512::AID-ANIE1512>3.0.CO;2-Y.
[5] L. Kelland, The resurgence of platinum-based cancer chemotherapy, Nat. Rev. Cancer 7 (2007) 573–584, https://doi.org/10.1038/nrc2167.
[6] A. Bergamo, G. Sava, Ruthenium anticancer compounds: myths and realities of the emerging metal-based drugs, Dalton Trans. 40 (2011) 7817–7823, https://doi.org/10.1039/C0DT01816C.
[7] M. Shabbir, Z. Akhter, A.R. Ashraf, H. Ismail, A. Habib, B. Mirza, Nickel (II) and palladium (II) triphenylphosphine complexes incorporating tridentate Schiff base ligands: synthesis, characterization and biocidal activities, J. Mol. Struct. 1149 (2017) 720–726, https://doi.org/10.1016/j.molstruc.2017.08.050.
[8] Y. Li, Y. Li, N. Wang, D. Lin, X. Liu, Y. Yang, Q. Gao, Synthesis, DNA/BSA binding studies and in vitro biological assay of nickel (II) complexes incorporating tridentate aroylhydrazone and triphenylphosphine ligands, J. Biomol. Struct. Dyn. 38 (2020) 4977–4996, https://doi.org/10.1080/07391102.2019.1694995.
[9] M. Grover, B. Singh, M. Bakshi, S. Singh, Quantitative structure–property relationships in pharmaceutical research–part 1, Pharmaceut. Sci. Tech. 3 (2000) 28–35, https://doi.org/10.1016/S1461-5347(99)00214-X.
[10] J. Akhtar, A.A. Khan, Z. Ali, R. Haider, M.S. Yar, Structure-activity relationship (SAR) study and design strategies of nitrogen-containing heterocyclic moieties for their anticancer activities, Eur. J. Med. Chem. 125 (2017) 143–189, https://doi.org/10.1016/j.ejmech.2016.09.023.
[11] W.A. Wani, S. Prashar, S. Shreaz, S. Gomez-Ruiz, Nanostructured materials functionalized with metal complexes: in search of alternatives for administering

anticancer metallodrugs, Coord. Chem. Rev. 312 (2016) 67–98, https://doi.org/10.1016/j.ccr.2016.01.001.
[12] A.M. Montana, C. Batalla, The rational design of anticancer platinum complexes: the importance of the structure-activity relationship, Curr. Med. Chem. 16 (2009) 2235–2260, https://doi.org/10.2174/092986709788453087.
[13] K.A. Abu-Safieh, A.S. Abu-Surrah, H.D. Tabba, H.A. AlMasri, R.M. Bawadi, F. M. Boudjelal, L.H. Tahtamouni, Novel palladium (II) and platinum (II) complexes with a fluoropiperazinyl based ligand exhibiting high cytotoxicity and anticancer activity *in vitro*, J. Chem. 2016 (2016), https://doi.org/10.1155/2016/7508724.
[14] J.J. Fernández, A. Fernández, D. Vázquez-García, M. López-Torres, A. Suárez, N. Gómez-Blanco, J.M. Vila, Tetranuclear Complexes of PdII with Tridentate [C, N, O] and [O, N, O] Ligands: Synthesis, Reactivity and Structural Isomerism, Wiley Online Library, 2007.
[15] H. Mansuri-Torshizi, T. Srivastava, H. Parekh, M. Chitnis, Synthesis, spectroscopic, cytotoxic, and DNA binding studies of binuclear 2, 2′-bipyridine-platinum (II) and-palladium (II) complexes of meso-α, α'-diaminoadipic and meso-α, α'-diaminosuberic acids, J. Inorg. Biochem. 45 (1992) 135–148, https://doi.org/10.1016/0162-0134(92)80008-J.
[16] L. Zeng, P. Gupta, Y. Chen, E. Wang, L. Ji, H. Chao, Z.-S. Chen, The development of anticancer ruthenium(ii) complexes: from single molecule compounds to nanomaterials, Chem. Soc. Rev. 46 (2017) 5771–5804, https://doi.org/10.1039/C7CS00195A.
[17] A.K. Bytzek, G. Koellensperger, B.K. Keppler, C.G. Hartinger, Biodistribution of the novel anticancer drug sodium trans-[tetrachloridobis(1H-indazole)ruthenate (III)] KP-1339/IT139 in nude BALB/c mice and implications on its mode of action, J. Inorg. Biochem. 160 (2016) 250–255, https://doi.org/10.1016/j.jinorgbio.2016.02.037.
[18] S. Thota, D.A. Rodrigues, D.C. Crans, E.J. Barreiro, Ru(II) compounds: next-generation anticancer metallotherapeutics? J. Med. Chem. 61 (2018) 5805–5821, https://doi.org/10.1021/acs.jmedchem.7b01689.
[19] S. Chamberlain, H.D. Cole, J. Roque, D. Bellnier, S.A. McFarland, G. Shafirstein, TLD1433-mediated photodynamic therapy with an optical surface applicator in the treatment of lung cancer cells in vitro, Pharmaceuticals 13 (2020) 137, https://doi.org/10.3390/ph13070137.
[20] W. Han Ang, P.J. Dyson, Classical and non-classical ruthenium-based anticancer drugs: towards targeted chemotherapy, Eur. J. Inorg. Chem. 2006 (2006) 4003–4018, https://doi.org/10.1002/ejic.200690041.
[21] D. de Oliveira Silva, Perspectives for novel mixed diruthenium-organic drugs as metallopharmaceuticals in cancer therapy, Anti Cancer Agents Med. Chem. 10 (2010) 312–323, https://doi.org/10.2174/187152010791162333.
[22] M. Flamme, E. Clarke, G. Gasser, M. Hollenstein, Applications of ruthenium complexes covalently linked to nucleic acid derivatives, Molecules (Basel, Switzerland) 23 (2018) 1515, https://doi.org/10.3390/molecules23071515.
[23] A. Bergamo, L. Messori, F. Piccioli, M. Cocchietto, G. Sava, Biological role of adduct formation of the ruthenium(III) complex NAMI-A with serum albumin and serum transferrin, Investig. New Drugs 21 (2003) 401–411, https://doi.org/10.1023/a:1026243000320.
[24] A.P. Lima, F.C. Pereira, M.A.P. Almeida, F.M.S. Mello, W.C. Pires, T.M. Pinto, F. K. Delella, S.L. Felisbino, V. Moreno, A.A. Batista, Cytoxicity and apoptotic mechanism of ruthenium (II) amino acid complexes in sarcoma-180 tumor cells, PLoS One 9 (2014), e105865, https://doi.org/10.1371/journal.pone.0105865.
[25] A. Bergamo, A. Masi, P.J. Dyson, G. Sava, Modulation of the metastatic progression of breast cancer with an organometallic ruthenium compound, Int. J. Oncol. 33 (2008) 1281–1289.
[26] P. Vijayan, P. Viswanathamurthi, P. Sugumar, M.N. Ponnuswamy, M. D. Balakumaran, P.T. Kalaichelvan, K. Velmurugan, R. Nandhakumar, R. J. Butcher, Unprecedented formation of organo-ruthenium (II) complexes containing 2-hydroxy-1-naphthaldehyde S-benzyldithiocarbazate: synthesis, X-ray crystal structure, DFT study and their biological activities in vitro, Inorg. Chem. Front. 2 (2015) 620–639, https://doi.org/10.1039/C5QI00029G.
[27] S. Kapitza, M.A. Jakupec, M. Uhl, B.K. Keppler, B. Marian, The heterocyclic ruthenium (III) complex KP1019 (FFC14A) causes DNA damage and oxidative stress in colorectal tumor cells, Cancer Lett. 226 (2005) 115–121, https://doi.org/10.1016/j.canlet.2005.01.002.
[28] M.R. Maurya, A. Kumar, A.R. Bhat, A. Azam, C. Bader, D. Rehder, Dioxo-and oxovanadium (V) complexes of thiohydrazone ONS donor ligands: synthesis, characterization, reactivity, and antiamoebic activity, Inorg. Chem. 45 (2006) 1260–1269, https://doi.org/10.1021/ic050811+.
[29] M.A. Ali, A.H. Mirza, R. Fereday, R.J. Butcher, J.M. Fuller, S.C. Drew, L.R. Gahan, G.R. Hanson, B. Moubaraki, K.S. Murray, Synthetic, EPR spectroscopic, magnetic and X-ray crystallographic structural studies on copper (II) complexes of the tridentate N2S donor ligand formed from 6-methyl-2-formylpyridine and S-methyldithiocarbazate (Hmpsme), Inorg. Chim. Acta 358 (2005) 3937–3948, https://doi.org/10.1016/j.ica.2005.06.063.
[30] P. Vijayan, P. Viswanathamurthi, V. Silambarasan, D. Velmurugan, K. Velmurugan, R. Nandhakumar, R.J. Butcher, T. Silambarasan, R. Dhandapani, Dissymmetric thiosemicarbazone ligands containing substituted aldehyde arm and their ruthenium (II) carbonyl complexes with PPh_3/$AsPh_3$ as ancillary ligands: synthesis, structural characterization, DNA/BSA interaction and in vitro anticancer activity, J. Organomet. Chem. 768 (2014) 163–177, https://doi.org/10.1016/j.jorganchem.2014.06.026.
[31] K. Gupta, A.K. Sutar, Catalytic activities of Schiff base transition metal complexes, Coord. Chem. Rev. 252 (2008) 1420–1450, https://doi.org/10.1016/j.ccr.2007.09.005.
[32] Ş. Güveli, B. Ülküseven, Nickel (II)–triphenylphosphine complexes of ONS and ONN chelating 2-hydroxyacetophenone thiosemicarbazones, Polyhedron 30 (2011) 1385–1388, https://doi.org/10.1016/j.poly.2011.02.041.
[33] O. Tokgun, D.E. Karakas, S. Tan, E.R. Karagür, B. İnal, H. Akca, F. Durap, A. Baysal, M. Aydemir, Novel ruthenium and palladium complexes as potential anticancer molecules on SCLC and NSCLC cell lines, Chem. Pap. (2020) 1–10, https://doi.org/10.1007/s11696-020-01129-x.
[34] X. Liang, X. Zou, L. Tan, W. Zhu, Study on nucleic acid (CT-DNA and yeast tRNA) binding behaviors and cytotoxic properties of a heterodinuclear Ru (II)–Co (III) polypyridyl complex, J. Inorg. Biochem. 104 (2010) 1259–1266, https://doi.org/10.1016/j.jinorgbio.2010.08.006.
[35] W. Ben Ayed, A. Ben Said, A. Hamdi, A. Mokrani, Y. Masmoudi, I. Toukabri, I. Limayem, Y. Yahyaoui, Toxicity, risk factors and management of cisplatin-induced toxicity: a prospective study, J. Oncol. Pharm. Pract. 26 (2020) 1621–1629, https://doi.org/10.1177/1078155219901305.
[36] S.A. Aldossary, Review on pharmacology of cisplatin: clinical use, toxicity and mechanism of resistance of cisplatin, Biomed. Pharmacol. J. 12 (2019) 7–15, https://doi.org/10.13005/bpj/1608.
[37] F.M. Muggia, A. Bonetti, J.D. Hoeschele, M. Rozencweig, S.B. Howell, Platinum antitumor complexes: 50 years since Barnett Rosenberg's discovery, J. Clin. Oncol. 33 (2015) 4219–4226, https://doi.org/10.1200/JCO.2015.60.7481.
[38] L. Venanzi, 140. Tetrahedral nickel (II) complexes and the factors determining their formation. Part I. Bistriphenylphosphine nickel (II) compounds, J. Chem. Soc. (1958) 719–724, https://doi.org/10.1039/JR9580000719.
[39] J.C. Bailar Jr., H. Itatani, Hydridochlorobis (triphenylphosphine) platinum (II) and Some Related Compounds, Inorg. Chem. 4 (1965) 1618–1620, https://doi.org/10.1021/ic50033a019.
[40] R.A. Sanchez-Delgado, W. Lee, S.R. Choi, Y. Cho, M.-J. Jun, The chemistry and catalytic properties of ruthenium and osmium complexes. Part 5. Synthesis of new compounds containing arsine ligands and catalytic activity in the homogeneous hydrogenation of aldehydes, Transit. Met. Chem. 16 (1991) 241–244, https://doi.org/10.1007/BF01032844.
[41] M. Das, S. Livingstone, Metal chelates of dithiocarbazic acid and its derivatives. IX. Metal chelates of ten new Schiff bases derived from S-methyldithiocarbazate, Inorg. Chim. Acta 19 (1976) 5–10, https://doi.org/10.1016/S0020-1693(00)91065-X.
[42] S. Saint, Bruker AXS Inc., Bruker AXS Inc., Madison, Wisconsin, USA, Bruker AXS Inc, 2007.
[43] G. Kalaiarasi, R. Jain, H. Puschman, S.P. Chandrika, K. Preethi, R. Prabhakaran, New binuclear Ni (II) metallates containing ONS chelators: synthesis, characterisation, DNA binding, DNA cleavage, protein binding, antioxidant activity, antimicrobial and in vitro cytotoxicity, New J. Chem. 41 (2017) 2543–2560, https://doi.org/10.1039/C6NJ03516G.
[44] S. Zehra, T. Roisnel, F. Arjmand, Enantiomeric amino acid Schiff base copper (II) complexes as a new class of RNA-targeted metallo-intercalators: single X-Ray crystal structural details, comparative in vitro DNA/RNA binding profile, cleavage, and cytotoxicity, ACS Omega 4 (2019) 7691–7705, https://doi.org/10.1021/acsomega.9b00131.
[45] L. Tabrizi, P. McArdle, A. Erxleben, H. Chiniforoshan, Nickel (II) and cobalt (II) complexes of lidocaine: synthesis, structure and comparative in vitro evaluations of biological perspectives, Eur. J. Inorg. Chem. 103 (2015) 516–529, https://doi.org/10.1016/j.ejmech.2015.09.018.
[46] Y. Sun, S. Bi, D. Song, C. Qiao, D. Mu, H. Zhang, Study on the interaction mechanism between DNA and the main active components in *Scutellaria baicalensis* Georgi, Sensors Actuators B Chem. 129 (2008) 799–810, https://doi.org/10.1016/j.snb.2007.09.082.
[47] K. Mishra, H. Ojha, N.K. Chaudhury, Estimation of antiradical properties of antioxidants using DPPH assay: a critical review and results, Food Chem. 130 (2012) 1036–1043, https://doi.org/10.1016/j.foodchem.2011.07.127.
[48] A.M. Sarhan, S.A. Elsayed, M.M. Mashaly, A.M. El-Hendawy, Oxovanadium (IV) and ruthenium (II) carbonyl complexes of ONS-donor ligands derived from dehydroacetic acid and dithiocarbazate: synthesis, characterization, antioxidant activity, DNA binding and *in vitro* cytotoxicity, Appl. Organomet. Chem. 33 (2019), e4655, https://doi.org/10.1002/aoc.4655.
[49] I. Ali, W.A. Wani, K. Saleem, Empirical formulae to molecular structures of metal complexes by molar conductance, Synth. React. Inorg, Met.-Org., and Nano-Met. Chem. 43 (2013) 1162–1170, https://doi.org/10.1080/15533174.2012.756898.
[50] Y. Kaya, A. Erçağ, A. Koca, New square-planar nickel (II)-triphenylphosphine complexes containing ONS donor ligands: synthesis, characterization, electrochemical and antioxidant properties, J. Mol. Struct. 1206 (2020) 127653, https://doi.org/10.1016/j.molstruc.2019.127653.
[51] P. Kalaivani, S. Saranya, P. Poornima, R. Prabhakaran, F. Dallemer, V.V. Padma, K. Natarajan, Biological evaluation of new nickel (II) metallates: synthesis, DNA/protein binding and mitochondrial mediated apoptosis in human lung cancer cells (A549) via ROS hypergeneration and depletion of cellular antioxidant pool, Eur. J. Inorg. Chem. 82 (2014) 584–599, https://doi.org/10.1016/j.ejmech.2014.05.075.
[52] D. Anu, P. Naveen, N.P. Rath, M. Kaveri, Palladium (II) complexes containing substituted thiosemicarbazones. Synthesis, spectral characterization, X-ray crystallography, biomolecular interactions and in vitro cytotoxicity, J. Mol. Struct. 1206 (2020) 127703, https://doi.org/10.1016/j.molstruc.2020.127703.
[53] N.R. Pramanik, S. Ghosh, T.K. Raychaudhuri, S. Ray, R.J. Butcher, S.S. Mandal, Synthesis, characterization and crystal structure of oxomolybdenum (VI) and (IV) complexes of some tridentate ONS donor ligands, Polyhedron 23 (2004) 1595–1603, https://doi.org/10.1016/j.poly.2004.03.010.

[54] M.E. El-Afify, S.A. Elsayed, T.I. Shalaby, E.A. Toson, A.M. El-Hendawy, Synthesis, characterization, DNA binding/cleavage, cytotoxic, apoptotic, and antibacterial activities of V (IV), Mo (VI), and Ru (II) complexes containing a bioactive ONS-donor chelating agent, Appl. Organomet. Chem. (2020) e6082, https://doi.org/10.1002/aoc.6082.

[55] S. Pacigová, R. Gyepes, J. Tatiersky, M. Sivák, Interpretation of the multiple vanadium-oxygen bonds in the central VO $(\eta_2\text{-}O_2)^+$ group. Synthesis, structure, supramolecular interactions and DFT studies for complexes with 2, 2′-bipyridine, 1, 10-phenanthroline, pyrazinato (1−) and pyrazinamide ligands, Dalton Trans. (2008) 121–130, https://doi.org/10.1039/B711347A.

[56] S. Eğlence-Bakır, M. Şahin, B.Z. Salt, E. Tüzün, E.M. Kara, G. Atun, S. Çavuş, İ. Kızılcıklı, Palladium (II) complexes with thione and thioalkylated thiosemicarbazones: electrochemical, antimicrobial and thermogravimetric investigations, Spectrochim. Acta A Mol. Biomol. Spectrosc. 237 (2020) 118358, https://doi.org/10.1016/j.saa.2020.118358.

[57] S.K. Maiti, M. Kalita, A. Singh, J. Deka, P. Barman, Investigation of DNA binding and bioactivities of thioether containing Schiff base Copper (II), Cobalt (II) and Palladium (II) complexes: Synthesis, characterization, spectrochemical study, viscosity measurement, Polyhedron 184 (2020) 114559, https://doi.org/10.1016/j.poly.2020.114559.

[58] A.M. Fayed, S.A. Elsayed, A.M. El-Hendawy, M.R. Mostafa, Complexes of cis-dioxomolybdenum (VI) and oxovanadium (IV) with a tridentate ONS donor ligand: synthesis, spectroscopic properties, X-ray crystal structure and catalytic activity, Spectrochim. Acta A Mol. Biomol. Spectrosc. 129 (2014) 293–302, https://doi.org/10.1016/j.saa.2014.03.064.

[59] M.A. Ali, N.E.H. Ibrahim, R.J. Butcher, J.P. Jasinski, J.M. Jasinski, J.C. Bryan, Synthesis and characterization of some four-and five-coordinate copper (II) complexes of 6-methyl-2-formylpyridinethiosemicarbazone (HNNS) and the X-ray crystal structures of the $[Cu(NNS)(CH_3COO)(H_2O)]$ and $[Cu(HNNS)(H_2O)(SO_4)].H_2O$ complexes, Polyhedron 17 (1998) 1803–1809, https://doi.org/10.1016/S0277-5387(97)00531-7.

[60] S.A. Aboafia, S.A. Elsayed, A.K. El-Sayed, A.M. El-Hendawy, New transition metal complexes of 2, 4-dihydroxybenzaldehyde benzoylhydrazone Schiff base (H_2dhbh): synthesis, spectroscopic characterization, DNA binding/cleavage and antioxidant activity, J. Mol. Struct. 1158 (2018) 39–50, https://doi.org/10.1016/j.molstruc.2018.01.008.

[61] N. Dharmaraj, P. Viswanathamurthi, K. Natarajan, Ruthenium (II) complexes containing bidentate Schiff bases and their antifungal activity, Transit. Met. Chem. 26 (2001) 105–109, https://doi.org/10.1023/A:1007132408648.

[62] M. Begum, E. Zangrando, M. Sheikh, R. Miyatake, M. Howlader, M. Rahman, A. Ghosh, Bischelated complexes of a dithiocarbazate N, S Schiff base ligand: synthesis, characterization and antimicrobial activities, Transit. Met. Chem. 42 (2017) 553–563, https://doi.org/10.1007/s11243-017-0160-x.

[63] R. Karvembu, S. Hemalatha, R. Prabhakaran, K. Natarajan, Synthesis, characterization and catalytic activities of ruthenium complexes containing triphenylphosphine/triphenylarsine and tetradentate Schiff bases, Inorg. Chem. Commun. 6 (2003) 486–490, https://doi.org/10.1016/S1387-7003(03)00021-2.

[64] M. Mohapatra, V. Chakravortty, K. Dash, Cobalt (II) and cobalt (III) complexes with hexadentate dioxime Schiff base ligands, Polyhedron 8 (1989) 1509–1515, https://doi.org/10.1016/S0277-5387(00)80327-7.

[65] K. Nakamoto, Infrared and Raman Spectra of Inorganic and Coordination Compounds. Handbook of Vibrational Spectroscopy, John Wiley & Sons, 2009.

[66] H. Khaledi, H.M. Ali, M.M. Olmstead, Coordination behavior of three geometric isomers of indole-based S-benzyldithiocarbazone ligands towards nickel, zinc and cadmium divalent ions, Inorg. Chim. Acta 366 (2011) 233–240, https://doi.org/10.1016/j.ica.2010.11.008.

[67] R. Prabhakaran, S. Renukadevi, R. Karvembu, R. Huang, J. Mautz, G. Huttner, R. Subashkumar, K. Natarajan, Structural and biological studies of mononuclear palladium (II) complexes containing N-substituted thiosemicarbazones, Eur. J. Inorg. Chem. 43 (2008) 268–273, https://doi.org/10.1016/j.ejmech.2007.03.006.

[68] D. Mishra, S. Naskar, M.G. Drew, S.K. Chattopadhyay, Mononuclear and binuclear ruthenium (II) complexes with 4-(phenyl) thiosemicarbazone of benzaldehyde: a discussion on the relative stabilities of the four-membered and five-membered chelate rings formed by the ligand, Polyhedron 24 (2005) 1861–1868, https://doi.org/10.1016/j.poly.2005.05.018.

[69] A.M. Plutín, A. Alvarez, R. Mocelo, R. Ramos, O.C. Sánchez, E.E. Castellano, M.M. d. Silva, W. Villarreal, L. Colina-Vegas, F.R. Pavan, Structure/activity of PtII/N, N-disubstituted-N'-acylthiourea complexes: anti-tumor and anti-mycobacterium tuberculosis activities, J. Braz. Chem. Soc. 29 (2018) 1256–1267, https://doi.org/10.21577/0103-5053.20170222.

[70] M.M. Tamizh, K. Mereiter, K. Kirchner, B.R. Bhat, R. Karvembu, Synthesis, crystal structures and spectral studies of square planar nickel (II) complexes containing an ONS donor Schiff base and triphenylphosphine, Polyhedron 28 (2009) 2157–2164, https://doi.org/10.1016/j.poly.2009.04.021.

[71] Y. Kurt, A. Koca, M. Akkurt, B. Ülküseven, Iron (III) and nickel (II) complexes of O, N, N, O-chelating benzophenone thiosemicarbazone: electrochemistry and in situ spectroelectrochemistry, Inorg. Chim. Acta 388 (2012) 148–156, https://doi.org/10.1016/j.ica.2012.03.023.

[72] L.M. Fostiak, I. García, J.K. Swearingen, E. Bermejo, A. Castiñeiras, D.X. West, Structural and spectral characterization of transition metal complexes of 2-pyridineformamide N (4)-dimethylthiosemicarbazone, Polyhedron 22 (2003) 83–92, https://doi.org/10.1016/S0277-5387(02)01330-X.

[73] S.A. Elsayed, A.M. Noufal, A.M. El-Hendawy, Synthesis, structural characterization and antioxidant activity of some vanadium (IV), Mo (VI)/(IV) and Ru (II) complexes of pyridoxal Schiff base derivatives, J. Mol. Struct. 1144 (2017) 120–128, https://doi.org/10.1016/j.molstruc.2017.05.020.

[74] G. Ayyannan, M. Mohanraj, M. Gopiraman, R. Uthayamalar, G. Raja, N. Bhuvanesh, R. Nandhakumar, C. Jayabalakrishnan, New Palladium (II) complexes with ONO chelated hydrazone ligand: synthesis, characterization, DNA/BSA interaction, antioxidant and cytotoxicity, Inorg. Chim. Acta (2020) 119868, https://doi.org/10.1016/j.ica.2020.119868.

[75] S.A. Elsayed, I.S. Butler, D.F. Gilson, B.J. Jean-Claude, S.I. Mostafa, Synthesis, spectral characterization, and anticancer activity of 6-methylpyridine-2-carbaldehdyethiosemicarbazone and its complexes; crystal structure and DFT calculations of [Pd (mpyptsc) Cl]· DMSO, J. Coord. Chem. 67 (2014) 2711–2727, https://doi.org/10.1080/00958972.2014.942224.

[76] J.R. Gispert, Coordination Chemistry, Wiley-VCH, Weinheim, 2008.

[77] H. Chen, J.A. Parkinson, R.E. Morris, P.J. Sadler, Highly selective binding of organometallic ruthenium ethylenediamine complexes to nucleic acids: novel recognition mechanisms, J. Am. Chem. Soc. 125 (2003) 173–186, https://doi.org/10.1021/ja027719m.

[78] N. Johnson, J. Hoeschele, R. Rahn, Kinetic analysis of the in vitro binding of radioactive cis-and trans-dichlorodiammineplatinum (II) to DNA, Chem. Biol. Interact. 30 (1980) 151–169, https://doi.org/10.1016/0009-2797(80)90122-2.

[79] V. Censi, A.B. Caballero, M. Perez-Hernandez, V. Soto-Cerrato, L. Korrodi-Gregorio, R. Perez-Tomas, M.M. Dell'Anna, P. Mastrorilli, P. Gamez, DNA-binding and in vitro cytotoxic activity of platinum (II) complexes of curcumin and caffeine, J. Inorg. Biochem. 198 (2019) 110749, https://doi.org/10.1016/j.jinorgbio.2019.110749.

[80] T. Watanabe, T. Umehara, M. Kohara, Therapeutic application of RNA interference for hepatitis C virus, Adv. Drug Deliv. Rev. 59 (2007) 1263–1276, https://doi.org/10.1016/j.addr.2007.03.022.

[81] C. Davey, L.T. Malek, P.F. Lens, F. Wielaard, Method for the Synthesis of Ribonucleic Acid (RNA), Google Patents, 1995.

[82] P. Kalaivani, R. Prabhakaran, F. Dallemer, P. Poornima, E. Vaishnavi, E. Ramachandran, V.V. Padma, R. Renganathan, K. Natarajan, DNA, protein binding, cytotoxicity, cellular uptake and antibacterial activities of new palladium (II) complexes of thiosemicarbazone ligands: effects of substitution on biological activity, Metallomics 4 (2012) 101–113, https://doi.org/10.1039/C1MT00144B.

[83] G. Barone, A. Terenzi, A. Lauria, A.M. Almerico, J.M. Leal, N. Busto, B. Garcia, DNA-binding of nickel (II), copper (II) and zinc (II) complexes: structure–affinity relationships, Coord. Chem. Rev. 257 (2013) 2848–2862, https://doi.org/10.1016/j.ccr.2013.02.023.

[84] A.K. Patra, M. Nethaji, A.R. Chakravarty, Synthesis, crystal structure, DNA binding and photo-induced DNA cleavage activity of (S-methyl-l-cysteine) copper (II) complexes of heterocyclic bases, J. Inorg. Biochem. 101 (2007) 233–244, https://doi.org/10.1016/j.jinorgbio.2006.09.018.

[85] A. Wolfe, G.H. Shimer, T. Meehan, Polycyclic aromatic hydrocarbons physically intercalate into duplex regions of denatured DNA, Biochemistry 26 (1987) 6392–6396, https://doi.org/10.1021/bi00394a013.

[86] M. Frugier, P. Schimmel, Subtle atomic group discrimination in the RNA minor groove, Proc. Natl. Acad. Sci. 94 (1997) 11291–11294, https://doi.org/10.1073/pnas.94.21.11291.

[87] M.T. Qashqoosh, Y.K. Manea, F.A. Alahdal, S. Naqvi, Investigation of conformational changes of bovine serum albumin upon binding with benzocaine drug: a spectral and computational analysis, BioNanoScience 9 (2019) 848–858, https://doi.org/10.1007/s12668-019-00663-7.

[88] K. Sakthikumar, R.V. Solomon, J.D. Raja, Spectro-electrochemical assessments of DNA/BSA interactions, cytotoxicity, radical scavenging and pharmacological implications of biosensitive and biologically active morpholine-based metal (ii) complexes: a combined experimental and computational investigation, RSC Adv. 9 (2019) 14220–14241, https://doi.org/10.1039/C8RA09218D.

[89] Y.-Q. Wang, H.-M. Zhang, G.-C. Zhang, W.-H. Tao, S.-H. Tang, Interaction of the flavonoid hesperidin with bovine serum albumin: a fluorescence quenching study, J. Lumin. 126 (2007) 211–218, https://doi.org/10.1016/j.jlumin.2006.06.013.

[90] J. Zhang, X. Gao, J. Huang, H. Wang, Probing the interaction between human serum albumin and 9-hydroxyphenanthrene: a spectroscopic and molecular docking study, ACS Omega 5 (2020) 16833–16840, https://doi.org/10.1021/acsomega.0c02031.

[91] R.K. Gupta, G. Sharma, R. Pandey, A. Kumar, B. Koch, P.-Z. Li, Q. Xu, D. S. Pandey, DNA/protein binding, molecular docking, and in vitro anticancer activity of some thioether-dipyrrinato complexes, Inorg. Chem. 52 (2013) 13984–13996, https://doi.org/10.1021/ic401662d.

[92] M. Bhattacharyya, U. Chaudhuri, R. Poddar, Evidence for cooperative binding of chlorpromazine with hemoglobin: equilibrium dialysis, fluorescence quenching and oxygen release study, Biochem. Biophys. Res. Commun. 167 (1990) 1146–1153, https://doi.org/10.1016/0006-291X(90)90643-2.

[93] J. Olmsted III, D.R. Kearns, Mechanism of ethidium bromide fluorescence enhancement on binding to nucleic acids, Biochemistry 16 (1977) 3647–3654, https://doi.org/10.1021/bi00635a022.

[94] G. Ayyannan, M. Mohanraj, G. Raja, N. Bhuvanesh, R. Nandhakumar, C. Jayabalakrishnan, New palladium (II) hydrazone complexes: synthesis, structure and biological evaluation, J. Photochem. Photobiol. B Biol. 163 (2016) 1–13, https://doi.org/10.1016/j.jphotobiol.2016.08.003.

[95] Y. Li, Y. Li, N. Wang, D. Lin, X. Liu, Y. Yang, Q. Gao, Synthesis, DNA/BSA binding studies and in vitro biological assay of nickel (II) complexes incorporating tridentate aroylhydrazone and triphenylphosphine ligands, J. Biomol. Struct. Dyn. (2020) 1–20, https://doi.org/10.1080/07391102.2019.1694995.

[96] M. Heydari, M.E. Moghadam, A. Tarlani, H. Farhangian, DNA as a target for anticancer phen-imidazole Pd (II) complexes, Biotechnol. Appl. Biochem. 182 (2017) 110–127, https://doi.org/10.1007/s12010-016-2314-2.
[97] M. Tripathi, C.G. Giri, D. Das, R. Pande, S. Sarkar, S. Giri, G. Roymahapatra, A. Sarkar, Synthesis, characterization and nucleic acid binding studies of mononuclear copper (II) complexes derived from azo containing O, O donor ligands, Nucleos. Nucleot. Nucl. 37 (2018) 563–584, https://doi.org/10.1080/15257770.2018.1508694.
[98] M. Tripathi, R. Khilari, Y. Thakur, B. Verma, M. Pardhi, R. Pande, Oxovanadium complex as potential nucleic acid binder, J. Macromol. Sci. A 54 (2017) 85–90, https://doi.org/10.1080/10601325.2017.1261620.
[99] K. Suntharalingam, R. Vilar, Interaction of metal complexes with nucleic acids, Annu. Rep. Sec. A (Inorg. Chem.) 107 (2011) 339–358, https://doi.org/10.1039/B918406F.
[100] J.R. Lakowicz, G. Weber, Quenching of protein fluorescence by oxygen. Detection of structural fluctuations in proteins on the nanosecond time scale, Biochemistry 12 (1973) 4171–4179, https://doi.org/10.1021/bi00745a021.
[101] N. Tayeh, T. Rungassamy, J.R. Albani, Fluorescence spectral resolution of tryptophan residues in bovine and human serum albumins, J. Pharm. Biomed. Anal. 50 (2009) 107–116, https://doi.org/10.1016/j.jpba.2009.03.015.
[102] A. Sułkowska, Interaction of drugs with bovine and human serum albumin, J. Mol. Struct. 614 (2002) 227–232, https://doi.org/10.1016/S0022-2860(02)00256-9.
[103] M.A. Husain, T. Sarwar, S.U. Rehman, H.M. Ishqi, M. Tabish, Ibuprofen causes photocleavage through ROS generation and intercalates with DNA: a combined biophysical and molecular docking approach, Phys. Chem. Chem. Phys. 17 (2015) 13837–13850, https://doi.org/10.1039/C5CP00272A.
[104] J. Mariam, P. Dongre, D. Kothari, Study of interaction of silver nanoparticles with bovine serum albumin using fluorescence spectroscopy, J. Fluoresc. 21 (2011) 2193–2199, https://doi.org/10.1007/s10895-011-0922-3.
[105] F. Samari, M. Shamsipur, B. Hemmateenejad, T. Khayamian, S. Gharaghani, Investigation of the interaction between amodiaquine and human serum albumin by fluorescence spectroscopy and molecular modeling, Eur. J. Inorg. Chem. 54 (2012) 255–263, https://doi.org/10.1016/j.ejmech.2012.05.007.
[106] E. Froehlich, J. Mandeville, C. Jennings, R. Sedaghat-Herati, H. Tajmir-Riahi, Dendrimers bind human serum albumin, J. Phys. Chem. B 113 (2009) 6986–6993, https://doi.org/10.1021/jp9011119.
[107] N. Wang, L. Ye, F. Yan, R. Xu, Spectroscopic studies on the interaction of azelnidipine with bovine serum albumin, Int. J. Pharm. 351 (2008) 55–60, https://doi.org/10.1016/j.ijpharm.2007.09.016.
[108] Y. Song, Y. Liu, W. Liu, F.A. Villamena, J.L. Zweier, Characterization of the binding of the Finland trityl radical with bovine serum albumin, RSC Adv. 4 (2014) 47649–47656, https://doi.org/10.1039/C4RA04616A.
[109] A. Petrovic, M. Zivanovic, R. Puchta, D. Cocic, A. Scheurer, N. Milivojevic, J. Bogojeski, Experimental and quantum chemical study on the DNA/protein binding and the biological activity of a rhodium (III) complex with 1, 2, 4-triazole as an inert ligand, Dalton Trans. 49 (2020) 9070–9085, https://doi.org/10.1039/D0DT01343A.
[110] B.-L. Fei, B. Yin, D.-D. Li, W.-S. Xu, Y. Lu, Enantiopure copper (II) complex of natural product rosin derivative: DNA binding, DNA cleavage and cytotoxicity, J. Biol. Inorg. Chem. 21 (2016) 987–996, https://doi.org/10.1007/s00775-016-1394-3.
[111] M.C. Cha, A. Lin, K.A. Meckling, Low dose docosahexaenoic acid protects normal colonic epithelial cells from araC toxicity, BMC Pharmacol. 5 (2005) 7, https://doi.org/10.1186/1471-2210-5-7.
[112] J. Singh, A.N. Srivastav, N. Singh, A. Singh, Stability constants of metal complexes in solution, in: Stability of Coordination Compounds, IntechOpen, 2019.
[113] A. Levina, A. Mitra, P.A. Lay, Recent developments in ruthenium anticancer drugs, Metallomics 1 (2009) 458–470, https://doi.org/10.1039/b904071d.
[114] E.S. Antonarakis, A. Emadi, Ruthenium-based chemotherapeutics: are they ready for prime time? Cancer Chemother. Pharmacol. 66 (2010) 1–9, https://doi.org/10.1007/s00280-010-1293-1.
[115] S.A. Elsayed, A.M. El-Hendawy, S.I. Mostafa, B.J. Jean-Claude, M. Todorova, I. S. Butler, Antineoplastic activity of new transition metal complexes of 6-methyl-pyridine-2-carbaldehyde-n (4)-ethylthiosemicarbazone: X-Ray crystal structures of [VO_2(mpETSC)] and [Pt(mpETSC) Cl], Bioinorg. Chem. Appl. 2010 (2010), https://doi.org/10.1155/2010/149149.
[116] C. Bézivin, S. Tomasi, F. Lohézic-Le Dévéhat, J. Boustie, Cytotoxic activity of some lichen extracts on murine and human cancer cell lines, Phytomedicine 10 (2003) 499–503, https://doi.org/10.1078/094471103322331458.
[117] M.A. Arafath, F. Adam, M.R. Razali, L.E.A. Hassan, M.B.K. Ahamed, A.M.S. Majid, Synthesis, characterization and anticancer studies of Ni (II), Pd (II) and Pt (II) complexes with Schiff base derived from N-methylhydrazinecarbothioamide and 2-hydroxy-5-methoxy-3-nitrobenzaldehyde, J. Mol. Struct. 1130 (2017) 791–798, https://doi.org/10.1016/j.molstruc.2016.10.099.
[118] P. Herst, T. Petersen, P. Jerram, J. Baty, M. Berridge, The antiproliferative effects of phenoxodiol are associated with inhibition of plasma membrane electron transport in tumour cell lines and primary immune cells, Biochem. Pharmacol. 74 (2007) 1587–1595, https://doi.org/10.1016/j.bcp.2007.08.019.
[119] W. Mahavorasirikul, V. Viyanant, W. Chaijaroenkul, A. Itharat, K. Na-Bangchang, Cytotoxic activity of Thai medicinal plants against human cholangiocarcinoma, laryngeal and hepatocarcinoma cells *in vitro*, BMC Complement. Altern. Med. 10 (2010) 55, https://doi.org/10.1186/1472-6882-10-55.
[120] M. Hosseini-Kharat, D. Zargarian, A.M. Alizadeh, K. Karami, M. Saeidifar, S. Khalighfard, L. Dubrulle, M. Zakariazadeh, J.-P. Cloutier, Z. Sohrabijam, *In vitro* and *in vivo* antiproliferative activity of organo-nickel SCS-pincer complexes on estrogen responsive MCF7 and MC4L2 breast cancer cells. Effects of amine fragment substitutions on BSA binding and cytotoxicity, Dalton Trans. 47 (2018) 16944–16957, https://doi.org/10.1039/C8DT03079K.
[121] V. Nikoletopoulou, M. Markaki, K. Palikaras, N. Tavernarakis, Crosstalk between apoptosis, necrosis and autophagy, Biochim. Biophys. Acta 1833 (2013) 3448–3459, https://doi.org/10.1016/j.bbamcr.2013.06.001.
[122] M. Pernar, Z. Kokan, J. Kralj, Z. Glasovac, L.-M. Tumir, I. Piantanida, D. Eljuga, I. Turel, A. Brozovic, S.I. Kirin, Organometallic ruthenium (II)-arene complexes with triphenylphosphine amino acid bioconjugates: synthesis, characterization and biological properties, Bioorg. Chem. 87 (2019) 432–446, https://doi.org/10.1016/j.bioorg.2019.03.048.
[123] M.S. D'Arcy, Cell death: a review of the major forms of apoptosis, necrosis and autophagy, Cell Biol. Int. 43 (2019) 582–592, https://doi.org/10.1002/cbin.11137.
[124] C. Gercel-Taylor, Diphenylamine assay of DNA fragmentation for chemosensitivity testing, in: Chemosensitivity: Volume II, Springer, 2005, pp. 79–82.
[125] T. Bal-Demirci, G. Congur, A. Erdem, S. Erdem-Kuruca, N. Özdemir, K. Akgün-Dar, B. Varol, B. Ülküseven, Iron (III) and nickel (II) complexes as potential anticancer agents: synthesis, physicochemical and structural properties, cytotoxic activity and DNA interactions, New J. Chem. 39 (2015) 5643–5653, https://doi.org/10.1039/C5NJ00594A.
[126] K.H. Kim, J.M. Sederstrom, Assaying cell cycle status using flow cytometry, Curr. Protoc. Mol. Biol. 111 (2015), https://doi.org/10.1002/0471142727.mb2806s111, 28.26.21-28.26.11.
[127] T. Chen, Y. Wong, Selenocystine induces apoptosis of A375 human melanoma cells by activating ROS-mediated mitochondrial pathway and p53 phosphorylation, Cell. Mol. Life Sci. 65 (2008) 2763, https://doi.org/10.1007/s00018-008-8329-2.
[128] J.P. Johnpeter, G. Gupta, J.M. Kumar, G. Srinivas, N. Nagesh, B. Therrien, Biological studies of chalcogenolato-bridged dinuclear half-sandwich complexes, Inorg. Chem. 52 (2013) 13663–13673, https://doi.org/10.1039/B918406F.
[129] G. Mühlgassner, C. Bartel, W.F. Schmid, M.A. Jakupec, V.B. Arion, B.K. Keppler, Biological activity of ruthenium and osmium arene complexes with modified paullones in human cancer cells, J. Inorg. Biochem. 116 (2012) 180–187, https://doi.org/10.1016/j.jinorgbio.2012.06.003.
[130] M. Malumbres, M. Barbacid, Cell cycle, CDKs and cancer: a changing paradigm, Nat. Rev. Cancer 9 (2009) 153–166, https://doi.org/10.1038/nrc2602.
[131] V. Velma, S.R. Dasari, P.B. Tchounwou, Low doses of cisplatin induce gene alterations, cell cycle arrest, and apoptosis in human promyelocytic leukemia cells, Biomark. Insights 11 (2016), https://doi.org/10.4137/BMI.S39445. BMI. S39445.
[132] P. Storz, Reactive oxygen species in tumor progression, Front Biosci. 10 (2005) 1881–1896, https://doi.org/10.2741/1667.
[133] S. Greay, D. Ireland, H. Kissick, A. Levy, M. Beilharz, T. Riley, C. Carson, Induction of necrosis and cell cycle arrest in murine cancer cell lines by Melaleuca alternifolia (tea tree) oil and terpinen-4-ol, Cancer Chemother. Pharmacol. 65 (2010) 877–888, https://doi.org/10.1007/s00280-009-1093-7.
[134] R. Subbegowda, T.O. Frommel, Aspirin toxicity for human colonic tumor cells results from necrosis and is accompanied by cell cycle arrest, Cancer Res. 58 (1998) 2772–2776.
[135] A. Ferro, T. Mestre, P. Carneiro, I. Sahumbaiev, R. Seruca, J.M. Sanches, Blue intensity matters for cell cycle profiling in fluorescence DAPI-stained images, Lab. Investig. 97 (2017) 615–625, https://doi.org/10.1038/labinvest.2017.13.
[136] M. Nüsse, W. Beisker, C. Hoffmann, A. Tarnok, Flow cytometric analysis of G1- and G2/M-phase subpopulations in mammalian cell nuclei using side scatter and DNA content measurements, Cytom. J. Int. Soc. Anal. Cytol. 11 (1990) 813–821, https://doi.org/10.1002/cyto.990110707.